Title: Towards a global deep learning model for daily soil CO_2 efflux

Valerie Smykalov vds5105@psu.edu [1], Ben Bond-Lamberty bondlamberty@pnnl.gov [2], Rodrigo Vargas rvargas@udel.edu [3,4], Li Li lxl35@psu.edu [1]

[1]Penn State University, University Park, PA
[2]Pacific Northwest National Laboratory, Joint Global Change Research Institute, College Park, MD, USA
[3]Department of Plant & Soil Sciences, University of Delaware, Newark, Delaware, USA
[4]School of Life Sciences, Arizona State University, Tempe, Arizona, USA

This is a non-peer-reviewed preprint submitted to EarthArXiv. This manuscript has been submitted to Global Biogeochemical Cycles for peer review.

Towards a global deep learning model for daily soil CO_2 efflux

Valerie Smykalov[1], Ben Bond-Lamberty[2], Rodrigo Vargas[3,4], Li Li[1]

[1]Penn State University, University Park, PA
[2]Pacific Northwest National Laboratory, Joint Global Change Research Institute, College Park, MD, USA
[3]Department of Plant & Soil Sciences, University of Delaware, Newark, Delaware, USA
[4]School of Life Sciences, Arizona State University, Tempe, Arizona, USA

Corresponding author: Li Li lxl35@psu.edu, Valerie Smykalov vds5105@psu.edu

Key Points:

1. We trained a deep learning model to predict daily soil CO_2 efflux using fine temporal resolution data from 82 diverse sites across the globe;
2. The model performed best in temperate mesic ecosystems with cyclical data patterns driven by seasonal temperature variations;
3. The model performed poorly at sites with little data and noncyclical temporal patterns, and struggled to capture pulses and seasonal peaks/troughs.

Abstract. Soil CO_2 efflux, the largest flux of CO_2 to the atmosphere, is expected to rise globally under climate change. Its magnitude and temporal variability are highly uncertain, and daily-scale models capturing rapid changes to environmental drivers remain rare. We used a global database of soil CO_2 efflux (total observations = 7,797,535 from 2002-2020) to train a deep learning model (Long Short-Term Memory, LSTM) to predict daily soil CO_2 efflux in 82 sites across gradients of climate, soil type, and land cover. The model achieved a median train and test Nash Sutcliffe Efficiency (NSE) of 0.54 and 0.02, respectively, and Kling Gupta Efficiency (KGE) of 0.67 and 0.30, respectively. The model performed well (NSE > 0.5 and KGE > 0.3) at about one-third of sites, mainly in temperate mesic ecosystems (where most training sites were located) with cyclical data patterns driven by temperature. The model performed poorly at sites with little data and noncyclical temporal patterns, mostly at extreme climates including arid, Arctic/boreal, and tropical ecosystems. The model struggled to capture soil CO_2 efflux pulses and peaks/troughs, highlighting the challenges of modeling extremes in time series. Our results demonstrate that LSTM models can leverage existing data to generate synthetic daily datasets, particularly for temperate mesic regions, but also underscore the challenges of learning relationships from a spatially biased dataset. To improve model performance, future data collection should prioritize 1) historically underrepresented ecosystems with variable temperature relationships; 2) conditions under extreme weather events that may become disproportionally impactful in a warming climate.

1. INTRODUCTION

Soil CO_2 efflux, often referred to as soil respiration, is the flux of CO_2 between soil and the atmosphere driven by subsurface heterotrophic and autotrophic respiration and chemical weathering reactions (Rey, 2015). Annual soil CO_2 efflux reaches 75–100 Pg C yr^{-1}, making it the largest flux of CO_2 to the atmosphere and the second largest terrestrial carbon flux behind

photosynthesis (Hashimoto et al., 2023). Soil CO_2 efflux can determine net terrestrial-atmospheric carbon balances from ecosystem (Desai et al., 2022) to global scales (Ballantyne et al., 2017; Metz et al., 2023) and is rising under global warming (Arora et al., 2013; Hashimoto et al., 2023; Lei et al., 2021). However, the magnitude and spatial-temporal variation of this rise has remained highly uncertain (Bond-Lamberty, 2018; Bond-Lamberty et al., 2016; Nissan et al., 2023; Varney et al., 2022). It remains unclear to what degree we will experience net soil carbon losses under climate change (van Gestel et al., 2018).

Many global models use bottom-up approaches, in which soil CO_2 efflux is predicted from empirical (e.g., Schlesinger, 1977), statistical (e.g., Bond-Lamberty & Thomson, 2010), or machine learning-inferred (e.g., Warner et al., 2019) relationships based on drivers such as temperature and precipitation (Raich et al., 2002). Global soil CO_2 efflux is usually estimated using annual scale data (Bond-Lamberty et al., 2024; Hashimoto et al., 2023), which has greatly advanced our understanding of its spatial-temporal patterns and sensitivities to environmental drivers. However, annual-scale data suffers from challenges including the temporal bias of measurements towards warmer seasons (Burton et al., 2004; Chang et al., 2009; Duiker & Lal, 2000; Janssens et al., 1998), nonlinearity in relationships with drivers (Jian et al., 2018), and spatial (Luo & Zhou, 2006; Song et al., 2013; Wang et al., 2021; Zhang et al., 2023; Zhao et al., 2017) and/or temporal non-stationarity (Bond-Lamberty et al., 2019; Vargas et al., 2010). Annual soil CO_2 efflux data are also known to be highly spatially biased (Bond-Lamberty et al., 2024; Stell et al., 2021; Xu & Shang, 2016), creating a further source of error. Perhaps unsurprisingly, estimates of global annual soil CO_2 efflux between different global models can differ dramatically, making this flux one of the most uncertain in global carbon cycle models (Hashimoto et al., 2023; Nissan et al., 2023; Varney et al., 2022).

Developing models at finer temporal scales has the potential to help reduce uncertainties in the global carbon cycle (Friedlingstein et al., 2024) by lowering the bias of coarser temporal measurements and by yielding more accurate understandings of the relationships between soil CO_2 efflux and drivers such as temperature, soil moisture, and vegetation at sub-annual scales (Jian et al., 2018). Jian et al. (2018) found notable differences in the magnitude of global soil CO_2 efflux between models constrained with annual, monthly, and daily data, with the use of monthly data reducing annual predictions by 7.43–9.46 Pg C, and daily-scale data by a further 1.82 Pg C. However, statistical models at such sub-annual scales remain uncommon (Hashimoto et al., 2015; Jian et al., 2018, 2022; Raich et al., 2002; Raich & Potter, 1995), and daily-scale global statistical models are rare (Adachi et al., 2017; Jian et al., 2018).

Acquisition of soil CO_2 efflux data has substantially advanced in recent decades with the technological advance of automated chambers enabling high-frequency, continuous measurements (Bond-Lamberty et al., 2024; Goulden & Crill, 1997; Irvine & Law, 2002; Rayment & Jarvis, 1997; Vargas et al., 2011). These datasets have enabled major advances in understanding the drivers of soil CO_2 efflux on seasonal, daily, and sub-daily scales (e.g., Carbone & Vargas, 2008; Gaumont-Guay et al., 2014; Misson et al., 2010; Thomey et al., 2011; Vargas et al., 2011; Vargas & Allen, 2008). These data have been compiled into a global database called COSORE with sites

covering gradients of climate, land cover, and soil types (Bond-Lamberty et al., 2020), enabling large-scale syntheses (e.g., Anjileli et al., 2021).

In addition to advances in data collection, deep learning has emerged as a powerful tool for inferring relationships between input and output variables by learning simultaneously from data in many sites under diverse conditions (Fang et al., 2022; Kratzert et al., 2019; Zhi et al., 2023). Although deep learning models alone cannot be used to gain an understanding of underlying processes (Perry et al., 2022), they have become increasingly applied in earth sciences for large-scale predictions of, for example, soil moisture (Fang et al., 2017), stream flow (Feng et al., 2020), stream dissolved oxygen (Zhi et al., 2023), rainfall-runoff relationships (Kratzert et al., 2018), and floods (Nearing et al., 2024). The Long Short-Term Memory (LSTM) model, a recurrent neural network model that can retain temporal information, has emerged as a powerful deep learning model for time series prediction (Hochreiter & Schmidhuber, 1997). It has been used to predict half-hourly-scale soil CO_2 efflux in dryland ecosystems (Jiang et al., 2022) and daily-scale ecosystem respiration in the Western United States (Chen et al., 2021).

Given these recent advances in data collection and deep learning models, we ask the following questions: (1) can we train a single deep learning model for daily soil CO_2 efflux in sites across gradients of climate and land cover type? (2) What are the dominant drivers of model performance? Based on previous work on the drivers of soil CO_2 efflux (Jiang et al., 2022; Warner et al., 2019), the impact of data bias (Bond-Lamberty et al., 2024; Stell et al., 2021; Xu & Shang, 2016), and the challenges of modeling hot moments (Bernhardt et al., 2017; McClain et al., 2003; Savage et al., 2014; Vargas et al., 2018; Wutzler et al., 2020), we hypothesize that (1) the model will perform better in sites with many years of data and in temperate climates with strong responses to temperature; and (2) the model will perform poorly at sites with a relatively shorter time series of data and noncyclical, highly stochastic data patterns resulting from weak relationships with temperature.

2. METHODS

2.1. Data Acquisition

The COntinuous SOil REspiration (COSORE) database version 0.7 (Bond-Lamberty et al., 2020) was downloaded in June 2024 (https://github.com/bpbond/cosore/releases). We used 82 out of the 85 total sites in the database, with two sites only reporting methane measurements and one site outside of the temporal range of predictor data (Figure 1). The northern hemisphere is far more represented (Figure 1a). There are many represented International Geosphere-Biosphere Programme (IGBP) land cover types (Loveland et al., 2000) (Figure 1b), with the top three being deciduous broadleaf forests, evergreen needleleaf forests, and evergreen broadleaf forests. Many land cover types only have one or two representative sites.

The sites cover a wide range of the mean annual temperature and precipitation climate space, although fewer sites have cold and dry or wet and warm climates (Figure 1c). A Budyko plot (Budyko, 1974) (Figure 1d) shows potential evapotranspiration/precipitation (PET/P, the aridity index) versus evapotranspiration/precipitation (ET/P, the evaporative index). Most sites are

humid (PET/P < 1), but there is ample representation of arid sites (PET/P > 1). Open shrublands, grasslands, woody savannas, savannas, desert woodlands, and croplands emerge as water-limited land cover types. The database covers 2003-2020 (Figure 1e), with the temporal coverage of individual sites ranging from 1-10 years.

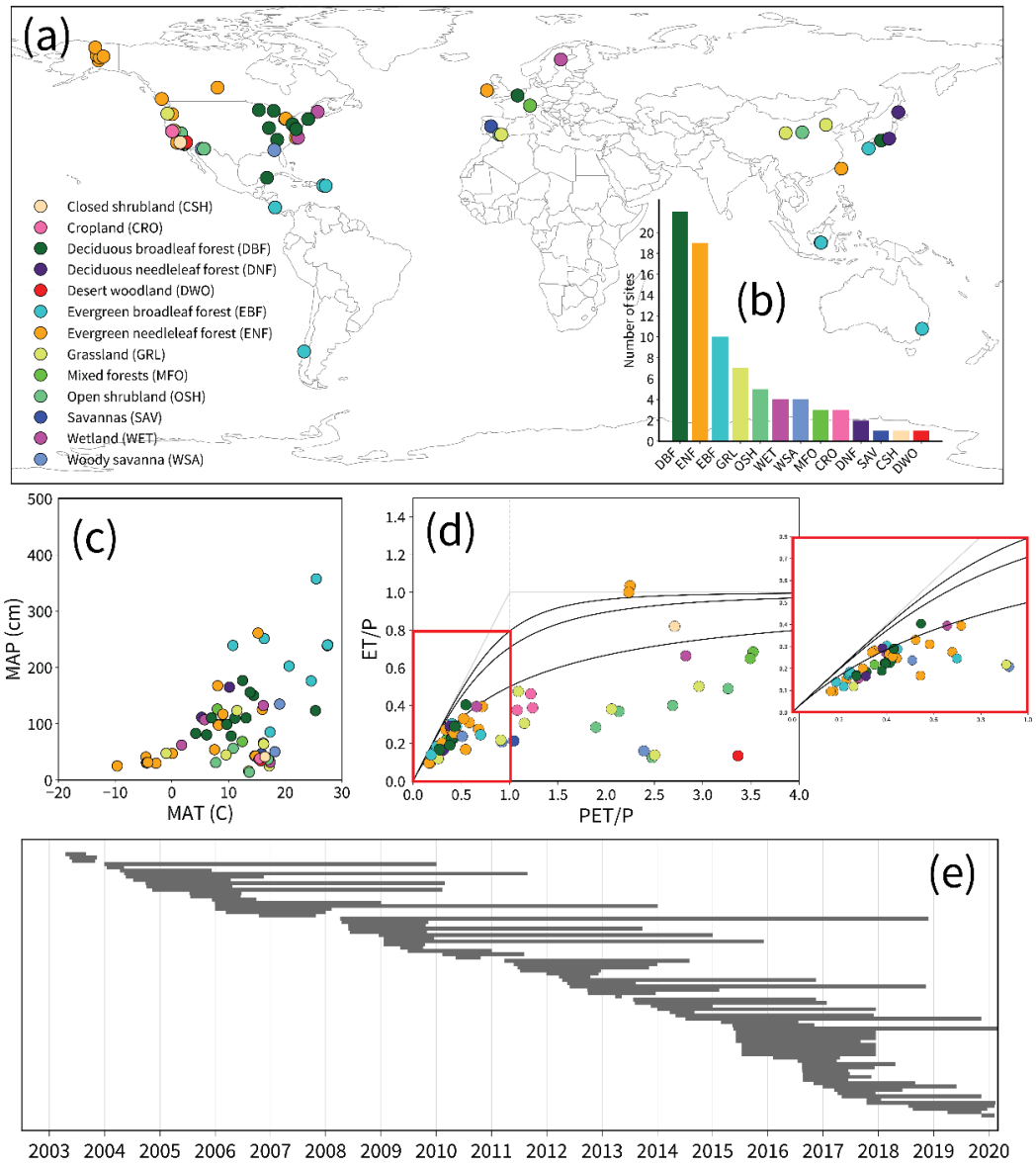

Figure 1. (a) Global spatial distribution of the 82 sites in the COSORE database used to train the model, color-coded by the International Geosphere-Biosphere Programme (IGBP) land cover classification of the site (Loveland et al., 2000); (b) Number of sites in each land cover type; (c) Sites plotted according to their mean annual temperature (MAT) versus mean annual precipitation (MAP); (d) Mean annual ET/P (evaporative index) versus mean annual PET/P (aridity index) (Budyko, 1974). The inset figure zooms in on sites with PET/P < 1, or humid sites. Sites with PET/P > 1 are water-limited or arid. Three Budyko curves with $\beta = 1$, 2, and 3 are plotted as references. (e) Time coverage of data in all sites in the COSORE database with available CO_2 data, ordered by the date of the first data entry.

COSORE includes static attributes such as latitude, longitude, elevation, and IGBP land cover classification for each site. However, the database lacks accompanying time series data for predictor variables at the same temporal scale as soil CO_2 efflux data. Previous work has shown that temperature (Kätterer et al., 1998; Kirschbaum, 1995; Lloyd & Taylor, 1994; Reichstein et al., 2000; Singh & Gupta, 1977), soil moisture (Carlyle & Than, 1988; Howard & Howard, 1993; Huang et al., 2020; Janssens et al., 2001; Norman et al., 1992; Raich & Potter, 1995), vegetation (Huang et al., 2020; Janssens et al., 2001; Norman et al., 1992; Raich & Potter, 1995), and soil properties (Haaf et al., 2021) are the main drivers of soil CO_2 efflux. We extracted time series of these predictor variables from remote sensing datasets from 01-01-2003 to 29-02-2020 using primarily Google Earth Engine (SI Table 1). Remote sensing data were extracted from a grid cell centered at each site's latitude and longitude with the finest possible scale for each remote sensing product. For example, for a data product with a 250 m resolution, we extracted data over a square cell with 250 m sides centered at the latitude/longitude of the site.

For temperature, we used MODIS daily daytime and nighttime land surface temperature (LST) at a spatial scale of 1000 m (https://doi.org/10.5067/MODIS/MOD11A1.061) and gap-filled and interpolated it to a daily temporal resolution (Shiff et al., 2021). We also used daily minimum and maximum air temperature from the Global Seamless High-resolution Temperature Dataset (GSHTD) at a spatial scale of 1000 m (Yao et al., 2023).

Hourly precipitation data were summed for each day from ERA5-Land at a spatial scale of about 11 km (https://doi.org/10.24381/cds.68d2bb30). We also used volumetric soil water content from 0-7 cm depth and 7-28 cm depth from the same mission, at the same spatial scale, and averaged for each day.

We used MODIS 8-day evapotranspiration (ET) and potential evapotranspiration (PET) at a spatial scale of 500 m (https://doi.org/10.5067/MODIS/MOD16A2.061) because some studies have found a significant correlation between ET and soil CO_2 efflux (Raich & Schlesinger, 1992). Quality flags were used for each data point to mask bad quality data, data from dead detectors, significant cloud cover, and the lowest confidence data.

For vegetation, we calculated normalized difference vegetation index (NDVI) using bands 3 and 4 of the USGS LANDSAT 7 Level 2, Collection 2, Tier 1 dataset at a spatial scale of 30 m (doi.org/10.5066/P9C7I13B). Negative NDVI values were removed, as they represent barren surface or water that did not make physical sense. We also used leaf area index (LAI) and fraction of photosynthetically activate radiation (FPAR) from MODIS at a spatial scale of 500 m and a temporal scale of 4 days.

All remote sensing products were cleaned using quality flags where available as described in their original data descriptors. Because the LSTM model requires all predictor data to be continuous, we used a simple linear interpolation method to gap-fill missing data to a daily resolution.

We extracted soil properties including soil organic content, sand, silt, clay content, and bulk density, as static site attributes from the SoilGrids2.0 global product (Poggio et al., 2021) at 250 m resolution. Mean annual precipitation and temperature were extracted at 1000 m resolution

from 1970-2000 from WorldClim version 2 (Fick & Hijmans, 2017). We also used elevation (meters above sea level), latitude, and longitude from the COSORE database as static site attributes.

Before model training, we first filtered out soil CO_2 efflux values from the raw target dataset above the 99th percentile or below the 1st percentile of data in each IGBP land cover type. Data are at a sub-daily scale (2 minutes to 1.5 hours), which we aggregated to the daily scale using the arithmetic mean for each day. We pre-processed the data by applying an arcsinh transformation, a commonly used pre-processing approach for data with negative or zero values (Burbidge et al., 1988; MacKinnon & Magee, 1990) which softens extreme values to help with model training. We used the equation $D^* = \ln(D + (1+D^2)^{1/2})$, where D^* represents transformed data and D represents raw data. We then applied a minimum/maximum scaling to all data using the global minimum and maximum (D_{min} and D_{max}) of each predictor, target, and static data across all datasets. For this we used the equation $D^{*0} = (D^* - D^*_{min}) / (D^*_{max} - D^*_{min})$, where D^{*0} represents scaled data.

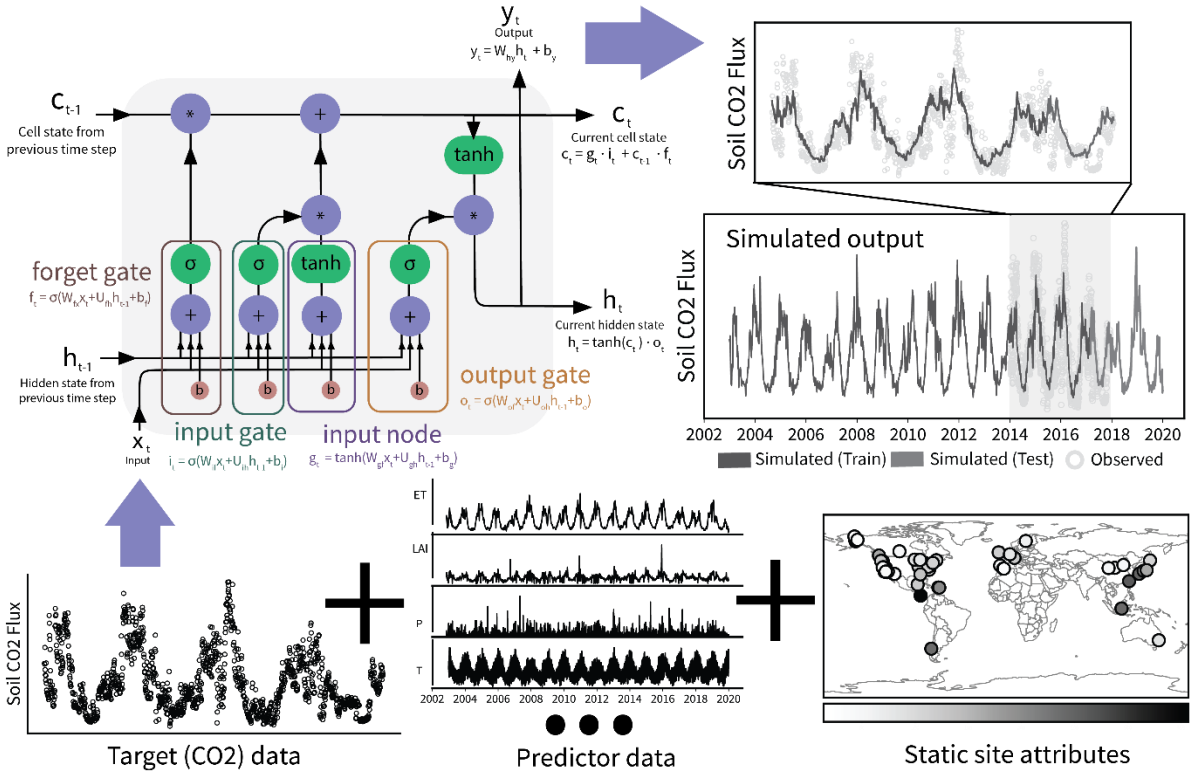

Figure 2. (a) Inputs to the LSTM model include the time series of target data (soil CO_2 efflux data), predictor data, and static site attributes for all sites. (b) Diagram of LSTM model structure. Inputs from the current time step x_t and the hidden state of the previous time step h_{t-1} (a "short-term" view of the state of the model) are carried through four gates: the forget gate, the input gate, the input node, and the output gate. The forget gate decides what information from the past to discard, the input gate and input node decide what information from the present to let through, and the output gate decides what information to output to future time steps. At each time step, the model outputs the hidden state of the model, the cell state of the model (a "long-term" view of the state of the model), and the desired output. (c) An example of a simulated output time series. The model can predict the entire time series of input predictor data, which in this model is from roughly 2003 to 2020.

2.2. Model Architecture

We used an LSTM model, a type of recurrent neural network that excels at resolving the problem of vanishing gradients and predicting sequential time series (Greff et al., 2017; Hochreiter & Schmidhuber, 1997; Shen, 2018). We chose to develop one single general model, following the common consensus about the power of "data synergy" effects: deep learning models perform better when they use data from diverse sites (Fang et al., 2022; Nearing et al., 2024; Nearing et al., 2021). Single LSTM models trained on many sites, often in the order of hundreds to even thousands of sites with daily data across decades, have been shown to perform better than models trained for individual sites and often outperform traditional process-based models that use parameters calibrated individually for every site (Nearing et al., 2021).

LSTM predicts each time step based on the cumulative influence of all previous time steps. Through a series of four model "gates," the model computes which data from the past to "remember" or carry forward for future predictive power and which data to "forget." (Figure 2). The input x includes time series of all predictor variables (daytime land surface temperature, daily minimum and maximum temperature, precipitation, soil moisture, evapotranspiration, potential evapotranspiration, leaf area index, NDVI, fraction of photosynthetically active radiation, and wind speed) and static site attributes (latitude, longitude, elevation, MAP, MAT, soil organic carbon content, sand, silt, and clay content, and soil bulk density) for each site.

At each time step t, the model outputs the cell state c_t (the "long-term" memory of the model), the hidden state h_t (the "short-term" memory of the model), and the final output y_t, which is the predicted soil CO_2 efflux at daily scale for each site (Figure 2). The error between the output y and the corresponding soil CO_2 efflux data is used to inform the tuning of model weights during each step of training (more details in the Supplementary Information Equations 1.1-1.8). We adapted code used in Zhi et al. (2023) to train our model, which implemented an LSTM architecture through the open source hydroDL code (https://github.com/mhpi/hydroDL) in PyTorch (Feng et al., 2020, 2021; Liu et al., 2022, 2024; Shen, 2018). The model was run using the CUDA Deep Neural Network library (cuDNN) to harness the computational power of the GPU. The model was run on a cluster with ½ slice of an NVIDIA A100 GPU (~3600 CUDA cores) and took around 1 hour to train.

2.3. Model Training and Evaluation

For all sites, we used the first 80% predictor and target (CO_2 efflux) time series data for training, and the last 20% for testing. Because the target data have different temporal coverage at different sites (Figure 1e), we used a flexible split scheme where data at each site was split at 80% of their total data points. We then ran a grid search to determine the optimal combination of hyperparameters. The optimal combination has a hidden state size of 128, a dropout rate of 0.2, a training-instance length of 30, and a random seed of 0. Mean squared error (MSE) was used as the objective function for model training and achieved a final loss of 0.003 after 200 training epochs.

The Nash Sutcliffe Efficiency (NSE) (Nash & Sutcliffe, 1970) and the Kling-Gupta Efficiency (KGE) (Gupta et al., 2009) were calculated for the train and test portion of each site to

evaluate model performance. NSE is a commonly used criterion for model fit in time series prediction based on the following equation:

$$NSE = 1 - \frac{\sum_{i=1}^{n}\left(R_{obs,i} - R_{sim,i}\right)^2}{\sum_{i=1}^{n}\left(R_{obs,i} - \overline{R_{obs}}\right)^2} \quad (1)$$

where $R_{obs,i}$ is the observed soil CO_2 efflux at each time step i, $R_{sim,i}$ is the simulated soil CO_2 efflux at each time step i, and $\overline{R_{obs}}$ is the mean of the observed time series. An NSE value above 0.0 indicates that the model fit outperformed the mean of the data, while an NSE value of 1 indicates perfect adherence to observed data.

KGE is another commonly used criterion of model fit for time series and is calculated using the following equation:

$$KGE = 1 - \sqrt{(r-1)^2 + \left(\frac{\sigma_{sim}}{\sigma_{obs}} - 1\right)^2 + \left(\frac{\mu_{sim}}{\mu_{obs}} - 1\right)^2} \quad (2)$$

where r is the linear correlation between observed and simulated soil CO_2 efflux, σ_{obs} and σ_{sim} are the standard deviation of the observed and simulated soil CO_2 efflux, and μ_{obs} and μ_{sim} are the means of the observed and simulated soil CO_2 efflux. A KGE above -0.41 indicates that model fit outperformed the mean of the data (Knoben et al., 2019), while a KGE value of 1 indicates perfect adherence to observed data.

We used both NSE and KGE because NSE is sensitive to extreme values and is therefore a good indicator of model prediction of pulses or seasonal peaks and troughs. In an LSTM model for stream dissolved oxygen with hundreds of sites, Zhi et al., (2023) used an NSE value of 0.7 as a threshold and NSE < 0.4 as thresholds for good and poor model performance, respectively. This model has much fewer sites and lower temporal coverage so we used NSE > 0.5 and KGE > 0.3 as the metric for good model performance, and NSE < 0.3 or KGE < 0.0 for poor model performance. The Pearson correlation coefficient (P_{corr}) between simulation output and observation data were also used to measure how well the model captured seasonal peaks, with P_{corr} = 1 indicating perfect adherence to data.

3.4. Data characteristics

We quantified target data characteristics and explored their relationships with model performance (Figure 3). Temporal patterns such as seasonality and the prevalence of spikes were quantified using autocorrelation analyses (Box & Jenkins, 1976). Data *smoothness* was defined as how much each data point differs from the preceding point, with data possessing many spikes being less smooth. Autocorrelation at a one-day offset can measure the data correlation with data from the day before and is a proxy for data smoothness, with smooth data possessing a high correlation to the preceding point.

Sites with highly seasonal trends tended to have a strong negative autocorrelation with their half-year (182-day) offset. Their data have diverging trends from the opposite season half a year

prior, leading to negative autocorrelation (close to -1) at a half-year offset. We call this metric data *seasonality*.

Data *cyclicity* measures how similar data patterns are from year to year, quantified by autocorrelation to a 365-day offset. More cyclical data with consistent interannual patterns have high correlation to the previous year's CO_2 efflux on the same day.

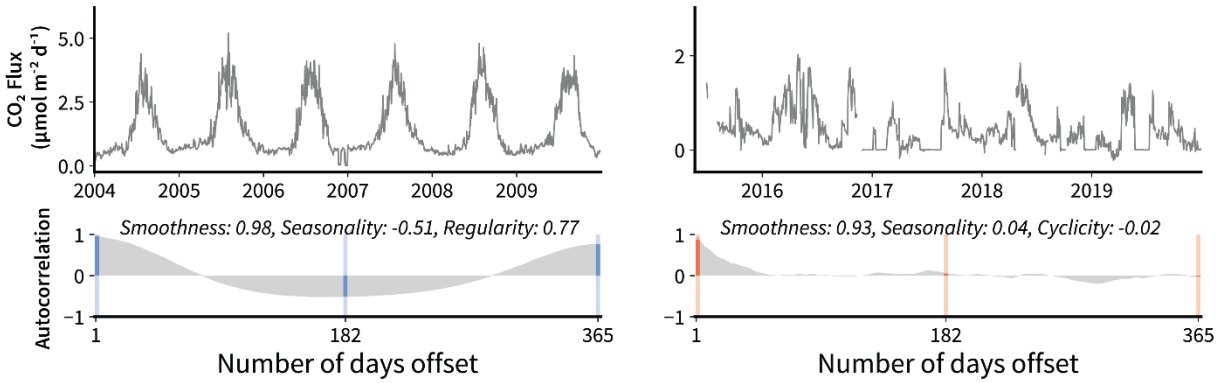

Figure 3 An autocorrelation analysis for a site with high smoothness, seasonality, and cyclicity (left) and vice versa (right). The top figure is a time series of observed soil CO_2 efflux, and the bottom figure is the autocorrelogram for the site (the Pearson correlation coefficient for the autocorrelation ranging from 1 day of offset to 365 days of offset). Smoothness was quantified using the extent of autocorrelation at a 1-day offset (leftmost highlighted line in each autocorrelation figure), seasonality was quantified using the extent of autocorrelation at a 182 (half-year) offset (center highlighted line in each autocorrelation figure), and cyclicity was quantified using the extent of autocorrelation at a 365-day offset (rightmost highlighted line in each autocorrelation figure). Each autocorrelation figure is labeled with the smoothness, seasonality, and cyclicity. The left site is from Gaumont-Guay et al. (2014) (10.1016/j.agrformet.2013.08.010), and the right site is from Wutzler et al. (2020) (10.5194/gi-9-239-2020), with the two sites located at (53.99, -105.12) and (39.94, -5.77), respectively.

3. RESULTS

3.1. Model Performance Overview

The model had a median (mean) train NSE of 0.54 (-0.05), with 57 sites (70%) having a train NSE value above 0.3 for good or fair performance. Median (mean) train KGE was 0.67 (0.54) and 76 sites (93%) had a train KGE above the threshold 0.0 for good or fair performance. The model had a median (mean) test NSE of 0.02 (-9.98), with 34 sites (41%) having a test NSE above 0.3. Model KGE was much better, with a median (mean) test KGE of 0.30 (0.06) and 58 sites (71%) having a test KGE above 0.0. Test NSE values had some notable outliers, with around 20% of sites having a test NSE < -5. Overall median (mean) train $P_{çorr}$ was 0.82 (0.74) and median (mean) test P_{corr} was 0.69 (0.55) across all sites.

Well-performing sites were defined as sites with test NSE > 0.5 and test KGE > 0.3, f*airly-performing sites* were defined as sites with 0.3 < test NSE < 0.5 and 0.0 > test KGE > 0.3, and *poorly-performing sites* were defined as sites with test NSE < 0.3 or test KGE < 0.0. Well-performing sites (n = 26) had a median (mean) NSE of 0.70 (0.72), median (mean) KGE of 0.79 (0.78), and median (mean) P_{corr} of 0.90 (0.89), showing a robust simulation of peaks. Fairly-performing sites (n = 8) had a median (mean) NSE of 0.35 (0.37), median (mean) KGE of 0.36

(0.38), and median (mean) P_{corr} of 0.75 (0.77), also indicating excellent reproduction of patterns. Poorly-performing sites (n = 48) had a median (mean) NSE of –1.48 (-17.50), median (mean) KGE of –0.02 (-0.38), and median (mean) P_{corr} of 0.37 (0.34), showing relatively poor adherence to seasonal peaks and troughs. Though we used NSE < 0.3 as one measure of poor model performance, 19% of sites in the "poor performance" category had KGE > 0.3, which indicates exceptional model performance. 75% of sites in the "fair performance" category had KGE > 0.3. In other words, NSE values were overall much lower than KGE values.

The model captured the generally sinusoidal dynamics at sites with good performance but often missed or underestimated spikes or seasonal maxima (Figure 4). At sites with fair performance, the model captured the general pattern in some cases while entirely missing the pattern in others. Sites with fair and poor performance often had less data coverage and less regular patterns across years. Interestingly, the model often overestimated soil CO_2 efflux at sites with poor performance (e.g. Third column, middle and last rows). In some cases, sites with the lowest number of data points had significantly different observed values in the testing portion (the last 20% of each site's data points) than the train portion, which could also account for outlier NSE and KGE values at these sites.

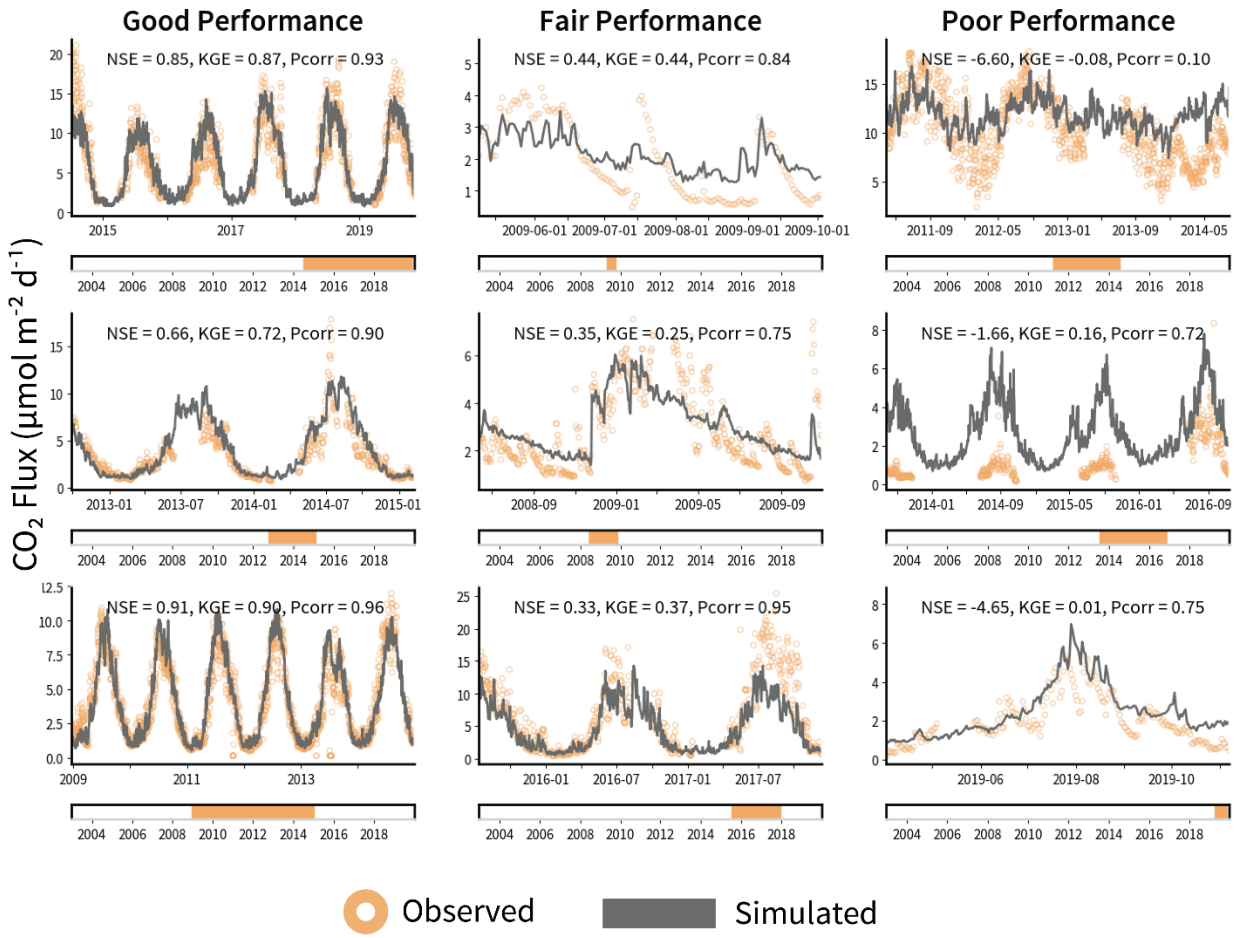

Figure 4. Three randomly selected sites from the group of well-performing sites (n=26, left column, test NSE > 0.3 and KGE > 0.0), fairly-performing sites (n = 17, middle column, test NSE > 0.0 and < 0.3 and KGE > -0.4 and < 0.0), and poorly-performing sites (n = 39, right column, test NSE < 0.0 or KGE < -0.4). Orange points are observed data, and the grey line is the model output. Bars at the bottom of each time series plot show the fraction of the total model time (2003 to 2020) covered by the data shown. Labeled NSE and KGE values are for the test (last 20% of data points) portion of each time series. Displayed sites with good model performance are from Arain (2016) (10.17190/AMF/1246152), Ataka et al. (2014) (10.1371/journal.pone.0108404), and Liang et al. (2017) (10.1038/sdata.2017.26), with coordinates at (42.635328, -80.557731), (34.79, 135.841), and (31.85, 131.3), respectively. Displayed sites with fair model performance are from Phillips et al. (2016) (10.1007/s10533-016-0204-x), Carbone et al. (2011) (10.1007/s00442-011-1975 and the Shale Hills Critical Zone Observatory, with coordinates at (44.565, -123.293), (34.00805556, -119.8102778), and (40.66541, -77.90475), respectively. Displayed sites with poor model performance are from Gutiérrez del Arroyo & Wood (2020) (10.1029/2019JG005353), Sihi et al. (2018) (10.1016/j.agrformet.2018.01.026) and Wu et al. (2016) (10.1071/RJ16023), with coordinates at (18.4075, -66.731389), (45.2041, -68.7402), and (40.46, 115.84), respectively.

All sites with good model performance had strong exponential relationships between temperature and CO_2 efflux, while at sites with fair and poor model performance, temperature and CO_2 efflux relationships were weak (Figure 5). The model captured the temperature-CO_2 efflux relationships for well-performing and fairly-performing sites but not for poorly-performing sites, often overshooting CO_2 efflux values over the same temperature range (e.g. third column, middle row in Figure 5).

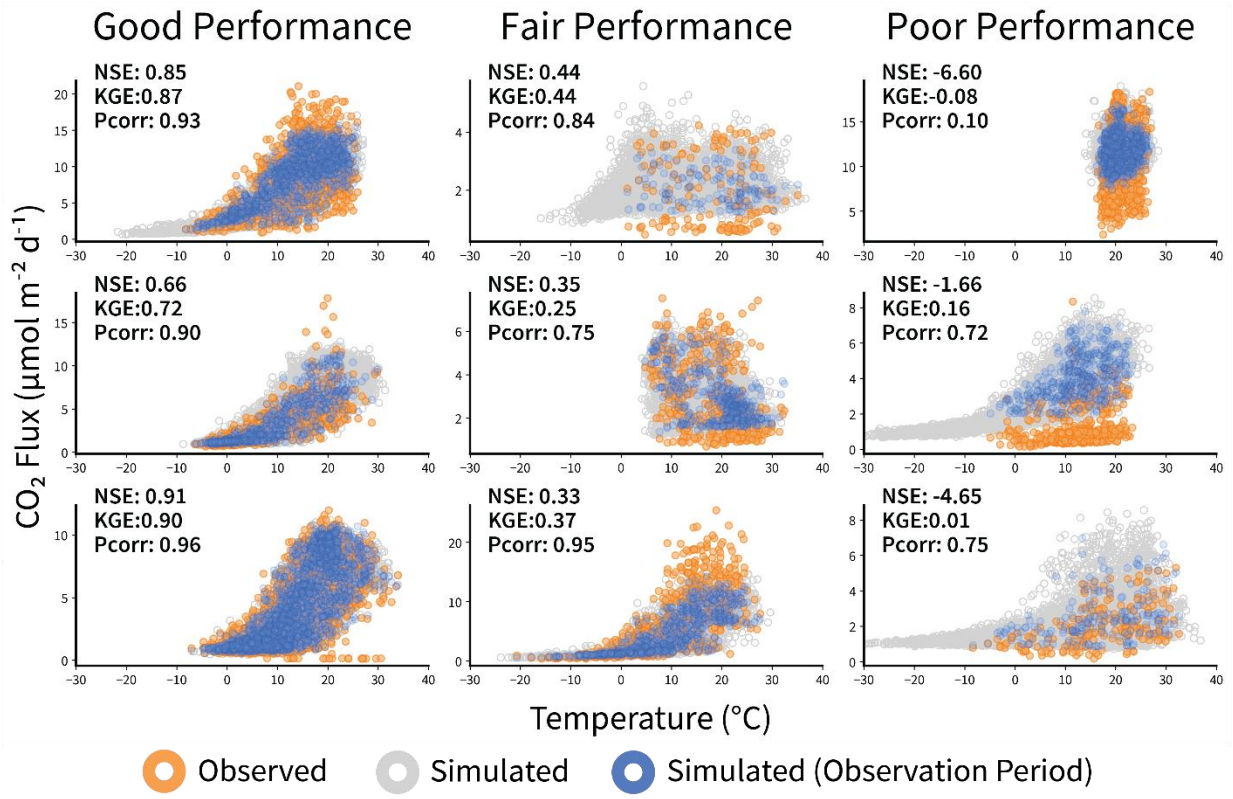

Figure 5. Temperature-CO_2 efflux relationships in three randomly sampled sites with good (left), fair (middle), and poor (right) model performance. Light grey points are model output, blue points are the model output at the observed data period, and orange points are observation data. Labeled NSE, KGE, and P_{corr} values correspond to the test portion of each dataset. In sites with good performance, the model captured the strong soil CO_2 efflux dependence on

temperature. In sites with fair and poor model performance, soil CO_2 efflux often did not have a strong dependence on temperature. Displayed sites are the same sites in Figure 4.

The model tended to underperform at the extremes of soil CO_2 efflux values (Figure 7c). We calculated NSE and KGE values for the top 5%, middle 90%, and bottom 5% of soil CO_2 efflux values across all sites. Notably, the model performed significantly more poorly in the top 5% (median NSE = -11.38, median KGE = -0.33) and bottom 5% (median NSE = -55.66, median KGE = -1.51) compared to the middle 90% (median NSE = 0.35, median KGE = 0.58). We also quantified model performance during spikes. Spikes were identified as any point with z-score > 3 or < -3 over a centered moving window of 30 days. Model performance was much worse for spikes compared to non-spike values (Figure 7d).

3.2. Model performance driven by data availability

Model performance often depended on data attributes including the number of data points and site representation in the same land cover type. Although the model performed well in many sites with few data points, there was a threshold-type relationship between the number of data points in individual sites and model performance. Sites with less than ~500 data points were much less likely to perform well (Figure 6a, b), indicating that having at least 1.5 years of data drastically improved model performance. Test KGE values correlated positively and significantly to the number of data points (r = 0.27, p = 0.016), but test NSE values were not significantly correlated with number of data points. When NSE outliers were removed using interquartile range (> Q3 + 1.5*IQR or < Q1 – 1.5*IQR, where Q3 is the third quartile of data, Q1 is the first quartile of data, and IQR is the interquartile range), NSE values just barely missed the threshold for a significant correlation (r = 0.24, p = 0.051). $P_{çorr}$ values also positively correlated to the number of data points (r = 0.30, p = 0.007), indicating that the number of data points is influential.

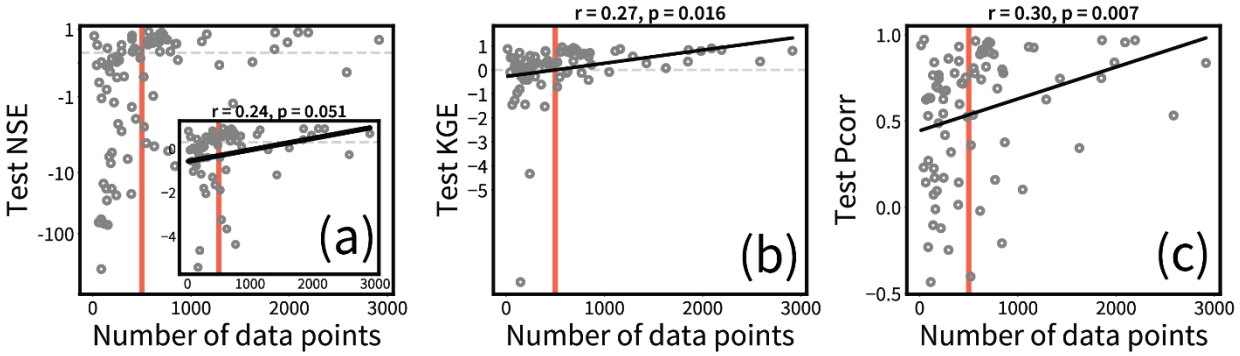

Figure 6 Test NSE (a), test KGE (b), and test P_{corr} (c) versus number of data points at each site. Inset plot in the left figure removes NSE outliers using the interquartile range method, revealing a significant correlation with number of data points. Correlation coefficients and p-values for relationships with significant correlations are above each plot. Sites with less than ~500 data points (Around 1.5 years of data, red vertical line) were much more likely to have bad performance (NSE < 0.5, KGE < 0.0), and P_{corr} < 0.5 (horizontal dashed grey line in each plot).

3.3. Model performance driven by climate

Climate was strongly linked to model performance. Sites with good model performance were primarily clustered in the 30-60° temperate latitudes (Figure 7a). Outside of this zone, median test NSE and test KGE were -1.21 and -0.13, respectively, compared to 0.33 and 0.38 inside the zone. The percentages of well-performing sites within and outside the temperate zone was 40% and 5%, respectively.

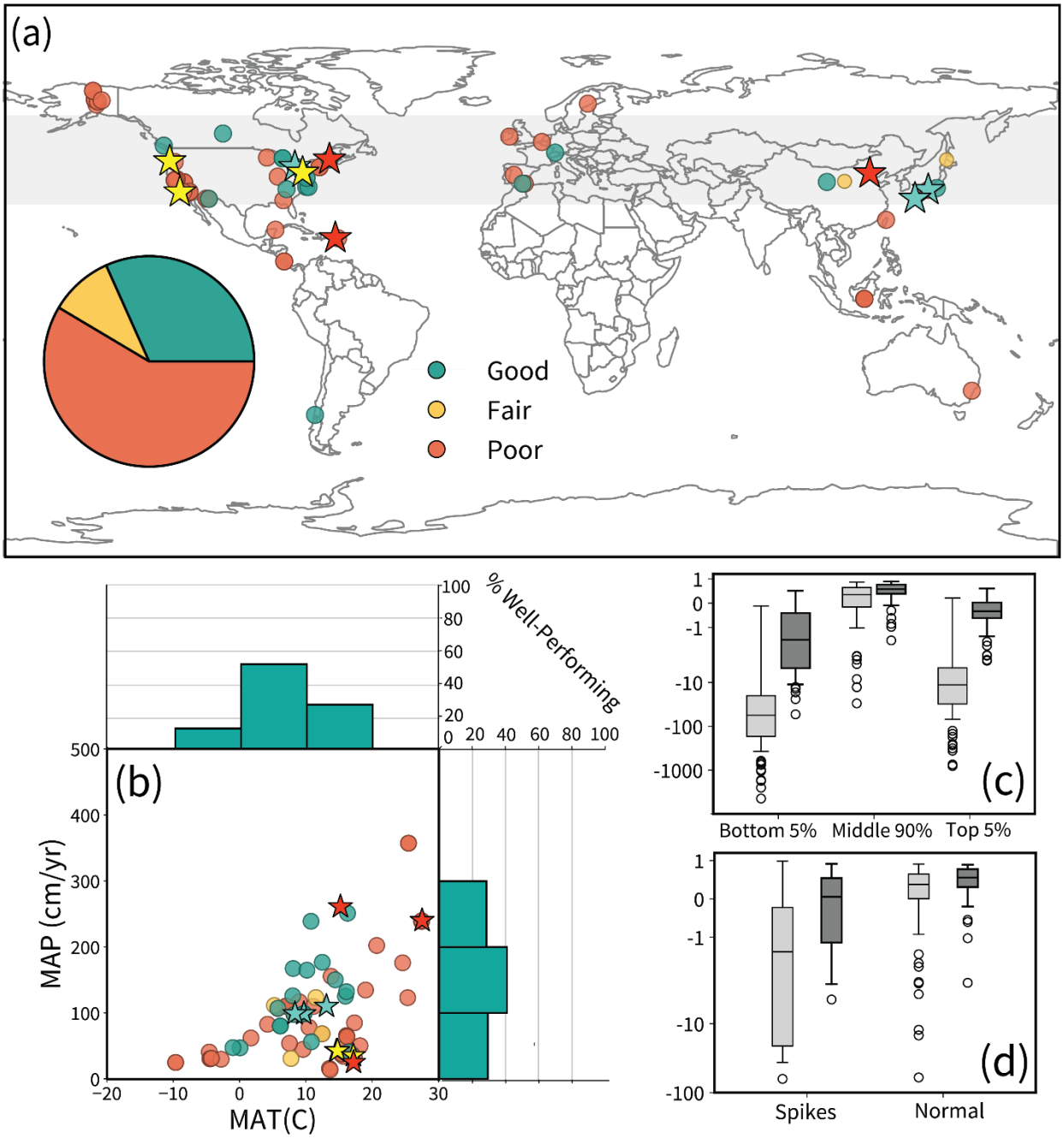

Figure 7. (a) Spatial distribution of sites with good model performance (green, test NSE > 0.3 and test KGE > 0.0), fair model performance (yellow, 0.0 < test NSE < 0.3 and -0.4 < test KGE < 0.0), and poor model performance (red, all other sites). The pie chart shows the relative proportion of sites with different performance. Notably, sites with good model performance are clustered around 30-60° latitude (light grey highlighted section) (b) Same sites in climate (MAT-MAP) space. Larger, brighter stars of each color correspond to the three randomly selected sites in

each category of performance in Figures 4 and 5. To the right and above each MAT-MAP plot is a bar plot of the % of well-performing site in each MAT or MAP interval. (c) NSE (dark grey) and KGE (light grey) distribution among spikes (left) and non-spikes (right). Spikes were quantified using points with z-score > 3 or < -3 along a 30-day moving window. Values are plotted on a symmetrical log scale for visual clarity. The model performed poorly for spikes. (d) NSE (dark grey) and KGE (light grey) distribution among the bottom 5% of soil CO_2 efflux values (left), the middle 90% of soil CO_2 efflux values (middle), and the top 5% of CO_2 flux values (right). Values are plotted on a symmetrical log scale for visual clarity. The model performed much worse at the highest (spikes) and lowest (troughs) soil CO_2 efflux values.

In general, sites at MAT and MAP's lower and upper extremes had relatively poor performance. The intermediate MAT ranges (0 to 15 C) had the highest percentage of sites with good performance (Figure 7b). Outside these temperate temperature ranges, the proportion of sites with good performance was low or zero. Correlating the number of sites in each temperature bin with median NSE and KGE in each bin or the percentage of well-performing sites in each bin did not produce a significant relationship, indicating that the better model performance in temperate MAP-MAT space is not explained by the fact that there are more sites at those climatic ranges.

A similar but weaker effect occurred in the breakdown of mean annual precipitation. Sites with MAP between 50 and 300 cm yr^{-1} generally had a higher percentage of sites with good model performance. The six land cover types with the lowest mean MAP (Desert woodland, Open shrubland, Cropland, Closed shrubland, Savannas, and Grassland) generally had low median test NSE (-30.07, 0.14, -0.40, -0.03, 0.03, and -0.28, respectively) and median test KGE (-0.37, 0.12, -0.29, -0.82, 0.01, and -0.12, respectively). Half of the arid sites (n = 13 out of 26) with MAP < 50 cm yr^{-1} had poor performance.

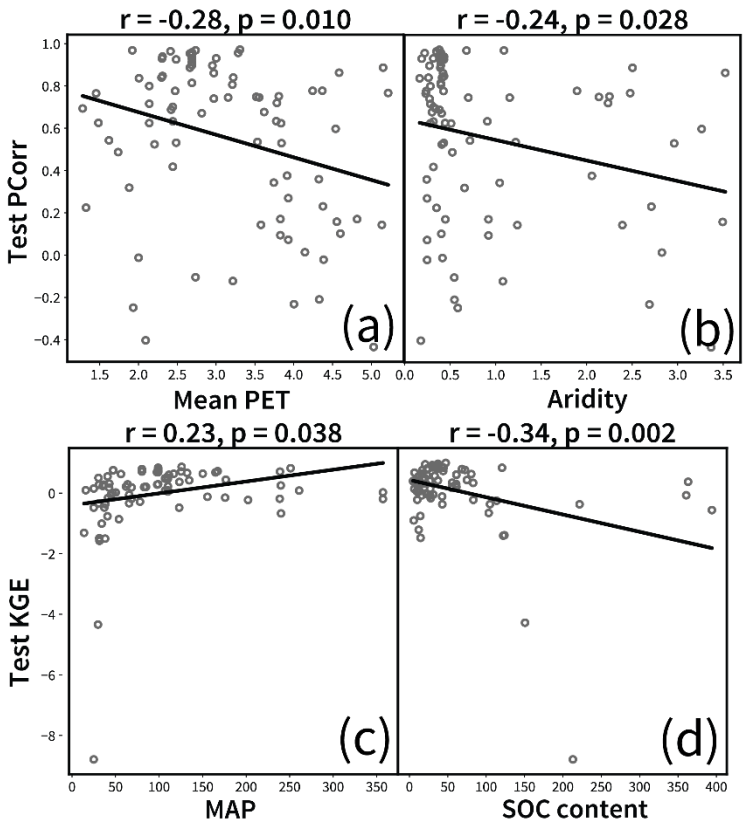

Figure 8: (a) Test P_{corr} versus mean PET; (b) Test P_{corr} versus aridity; (c) test KGE versus MAP; (d) Test KGE versus SOC content

Test P_{corr} was negatively correlated with multiple climatic attributes (Figure 8a,b), including mean PET ($r = -0.28$, $p = 0.010$) and aridity index (PET/P) ($r = -0.24$, $p = 0.028$), indicating that the model could capture the dynamics of the observed data better in sites with a relatively humid climate. Test KGE was also positively correlated to MAP ($r = 0.23$, $p = 0.038$) (Figure 8c). Correlating model performance with other site attributes revealed a negative correlation between test KGE and soil organic carbon (SOC) content ($r = -0.34$, $p = 0.002$) (Figure 8d), meaning that sites with higher SOC had poorer model performance.

3.4. Model performance driven by cyclic seasonal data patterns

Temporal patterns such as data smoothness (the prevalence of spikes), seasonality (how strongly CO_2 efflux responded to seasonal temperature variations), and cyclicity (degree of interannual similarity in CO_2 efflux dynamics) were quantified using autocorrelation analyses. Interestingly, data smoothness was not significantly correlated with any performance metric. Seasonality correlated significantly with test P_{corr} ($r = 0.41$, $p < 0.001$). This indicates that sites where CO_2 efflux are more seasonal or more responsive to temperature performed better. Finally, data cyclicity correlated strongly and significantly with test NSE ($r = 0.30$, $p = 0.014$), test KGE ($r = 0.33$, $p = 0.003$), and test P_{corr} ($r = 0.45$, $p < 0.001$), meaning that sites with similar soil CO_2 efflux patterns across years performed better (Figure 9).

Furthermore, the average absolute difference between mean summertime and mean wintertime soil efflux was 4.65 and 1.56 µmol m^{-2} d^{-1} at sites with good and poor performance, respectively (t-statistic = 5.16, $p < 0.001$). A wider data spread indicates higher seasonality, with strong summer peaks and wintertime lows in R_s. This suggests that the model can capture the larger difference between different seasons but does not do as well at sites where CO_2 efflux is relatively consistent. This further supports the idea that the model performs better at sites with highly seasonal soil CO_2 efflux.

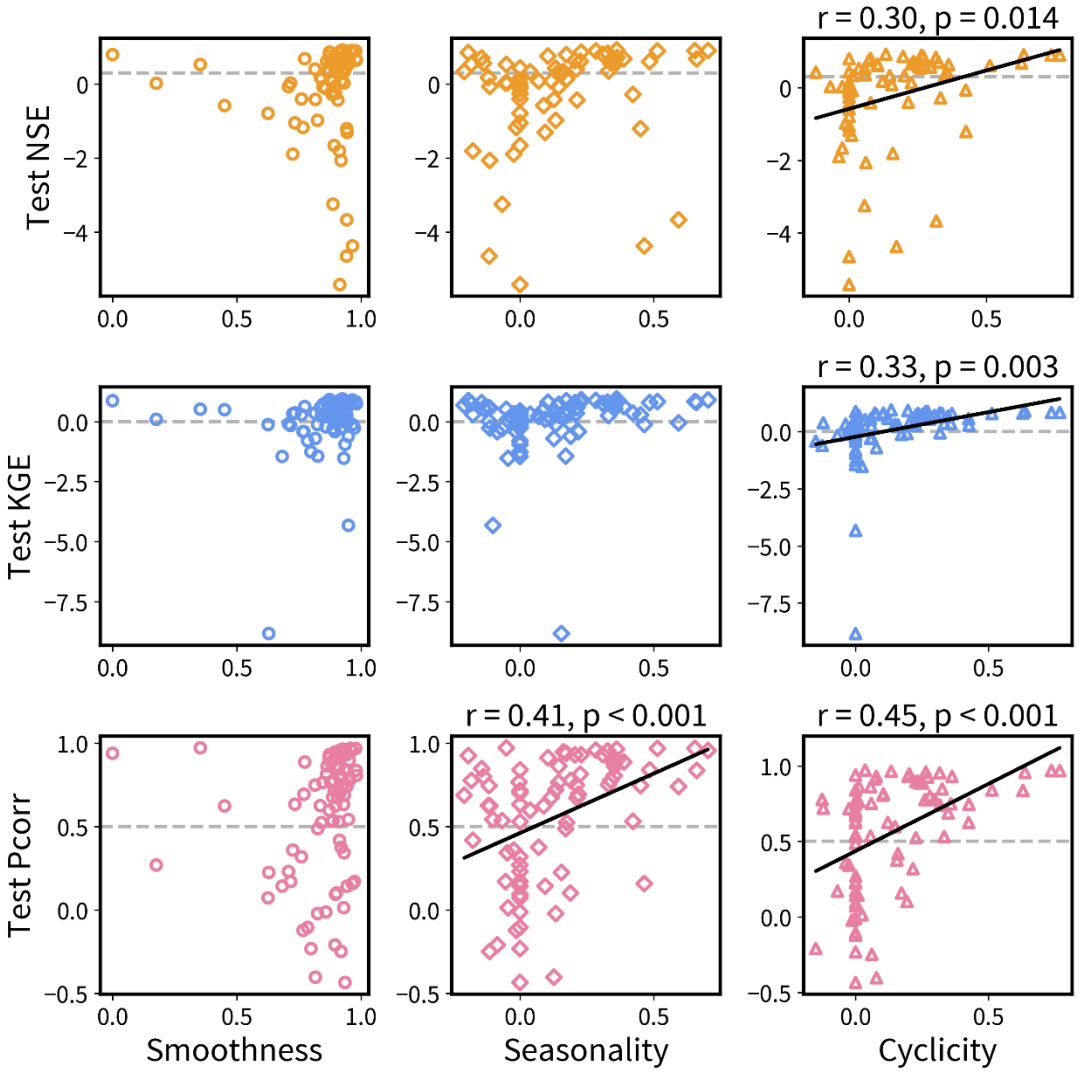

Figure 9. Correlations between smoothness (circles), seasonality (diamonds), and cyclicity (triangled) of data and test NSE (orange), test KGE (blue), and test Pearson correlation coefficient (pink). Significant correlations ($p < 0.05$) have labeled r and p values above the plot and plotted correlation lines.

4. DISCUSSION

Global estimation of soil CO_2 efflux has remained highly uncertain, and daily-scale models have the potential to reduce estimation uncertainty by using higher temporal resolution data and

inferring dynamics from daily to seasonal scales. As an important step in this direction, we leverage recent advances in continuous, high-frequency data acquisition and emergent deep learning models to develop a single deep learning model to predict daily soil CO_2 efflux in sites across gradients of climate, land cover, and soil properties (Reichstein et al., 2019). Our results largely support our hypotheses regarding when and where the model will perform well. They also raise fundamental questions about the transferability of daily dynamics and relationships learned from data-rich sites to data-poor sites, data availability, equity, and priorities for further data acquisition.

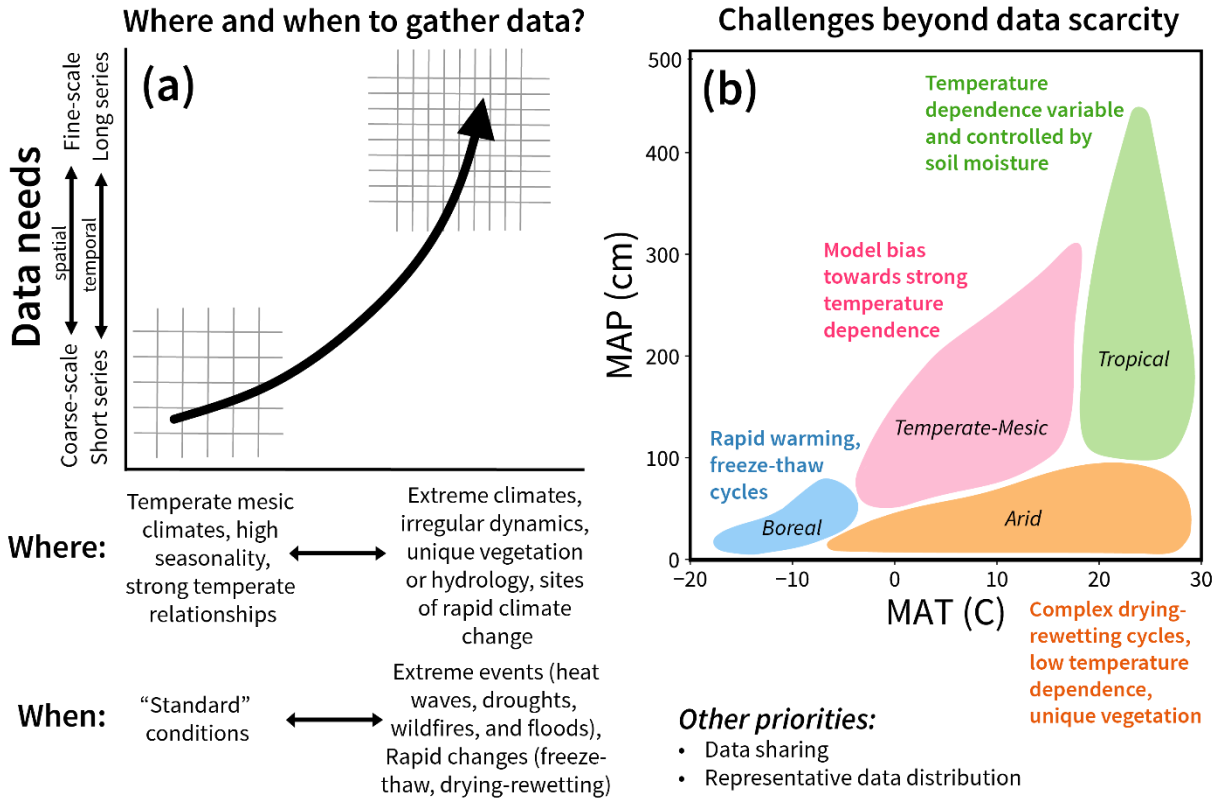

Figure 10. Overview of model challenges and further data needs recommended to improve future daily-scale models. (a) The most pressing data needs* are in climate at the high and low end of MAP and MAT spectrum, particularly those with unique hydrological (e.g., Wetlands and arid sites) characteristics or vegetation (e.g., Biocrusts) or and those experiencing rapid climate change, as well as during hot moments when soil CO_2 efflux is rapidly mobilized** (b) Challenges beyond data scarcity in each of four broad climate zones: temperate-mesic, boreal, arid, and tropical. Other priorities include data sharing and equitable data distribution across many climate types. *Note that more data is always better, but this represents where data collection efforts should be focused with the goal of correcting past inequalities.

4.1 How does the model compare to other models?

Deep learning models such as LSTM models are, by definition, data-driven, meaning they learn relationships between input and output variables based on training data without process-based knowledge. Naturally, the model will learn better with more training sites and longer data time series. Being "data greedy" is one of the major limitations of deep learning models such as

LSTM models (Shen et al., 2023). Compared to hundreds or even thousands of sites for streamflow and water quality data with multi-decadal coverage (Kratzert et al., 2023; Sterle et al., 2024), data here are sparse in terms of both the number of sites (82) and the temporal coverage within individual sites (0-10 years). As a result, overall model performance cannot rival those of LSTM models developed for hydrology and water quality predictions (Feng et al., 2021; Zhi et al., 2023).

The climate-driven model performance observed here generally aligns with insights learned from global models for annual soil CO_2 efflux (e.g., Jiang et al., 2024; Warner et al., 2019) as well as process-based Earth System Models (Guenet et al., 2024), which are most uncertain in arid/semi-arid, tropical, and cold regions, at the upper and lower ends of MAT and MAP where temperature relationships are weak and data tends to be much sparser. Our use of an unprecedentedly large (n = 7.8M) training dataset provides new information on what will be required to parameterize and assess robust models in biogeochemical and carbon-cycle domains (Reichstein et al. 2019). The struggle of reproducing hot moments has also been well-documented in previous studies (Bernhardt et al., 2017; McClain et al., 2003; Savage et al., 2014; Vargas et al., 2018; Wutzler et al., 2020). It is thus unsurprising that this model fared poorly at capturing the lowest and highest values across sites, but its challenges in this area provide interesting insights into both data and process-knowledge limitations that would be obscured using an annual-scale model.

4.2 Can the model extrapolate relationships learned from data-rich sites to data-poor sites?

The climatic distribution of COSORE sites is skewed toward countries with abundant access to scientific resources (Bond-Lamberty et al., 2024; Kim et al., 2022), reflecting a well-documented spatial bias in data acquisition (Stell et al., 2021; Xu & Shang, 2016). This is also true of ecological data more generally (Martin et al., 2012). Like the SRDB database of annual-scale soil CO_2 efflux data, COSORE overrepresents northern latitudes (30–60°) and temperate climates while underrepresenting Arctic regions, Central Asia, South America, Africa, Eastern Europe, Southeast Asia, Australia, and the Pacific islands. Data coverage is particularly sparse in climatic zones at the extremes of MAT and MAP, such as Arctic and arid ecosystems (e.g., closed shrublands, desert woodlands, and savannas), with limited site numbers and shorter data records.

Because of this data bias, the model mainly learned input-output relationships based on data biased toward temperate mesic sites with cyclic, seasonal patterns, which is where the model performed best. This is a common problem when training deep learning models on class-imbalanced datasets (Bauder et al., 2018; Johnson & Khoshgoftaar, 2019). In fact, all sites with good model performance had exponential, Arrhenius-type relationships between temperature and CO_2 efflux (Figure 6). The model then "extrapolated" such relationships to other sites. Such extrapolation worked well for sites with sparse data but temperate climates, where the model was able to capture dynamics well. However, when the model extrapolated such relationships to non-temperate/mesic sites where such relationships were weak or did not exist, it tended to overestimate soil CO_2 efflux, potentially because it overestimated the strength of temperature as a driver (Figure 6), leading to poor prediction.

555 This challenges the paradigm that temperature is the primary driver of soil CO_2 efflux
556 across the globe (e.g., Kirschbaum, 1995), which reflects insights from data-rich sites and has been
557 widely used to predict soil CO_2 efflux across the world. Many studies now show that Q_{10} has high
558 spatial and temporal variability (Chen et al., 2020; Meyer et al., 2018; Zhou et al., 2009), however,
559 implying that temperature dependence is regulated by a complex interplay of factors, particularly
560 in arid and tropical regions (e.g., Le & Vargas, 2024; Wood et al., 2013).
561
562 **4.3 Where and when should we prioritize data collection?**
563 Predicting dynamics requires model generalizability—the ability to extrapolate beyond the
564 training data. Unlike process-based models, deep learning models rely solely on patterns encoded
565 in the training data and require sufficient exposure to diverse input-output relationships to capture
566 temporal trends and spatial patterns. Because we cannot measure the response of soil CO_2 efflux
567 under every condition in every location, the training data we use in such models must represent
568 global diversity in dynamics, responses, and conditions.
569 Achieving meaningful representation is, however, more complex than simply adding data
570 (Villarreal et al., 2019; Villarreal & Vargas, 2021). For example, Stell et al. (2021) demonstrated
571 that expanding spatial coverage in a newer version of SDRB increased model uncertainty; model
572 performance only improved when data distribution optimized coverage of the covariate space. In
573 other words, greater data diversity for better model performance is achieved only when the
574 diversity is relatively balanced; otherwise, models will overfit to well-sampled space, time, and
575 conditions while failing in data-scarce regions and time periods (Bauder et al., 2018; Johnson &
576 Khoshgoftaar, 2019).
577 **Where?** To reduce data bias, we need to collect more data both by increasing the number of
578 sites and extending data duration and conditions at individual sites. Particular attention should be
579 devoted to sites at the upper and lower extremes of MAP and MAT where soil CO_2 efflux is more
580 likely to be regulated by factors other than temperature such as soil moisture. These regions are
581 important to prioritize because they are particularly susceptible to climate change (Bond-Lamberty
582 et al., 2024). Arctic or boreal regions have experienced warming at four times the rate of the rest
583 of the globe (Rantanen et al., 2022) and are highly vulnerable to shifts in vegetation and land cover
584 under climate change (Gonzalez et al., 2010), yet have extremely sparse measurements.
585 Furthermore, arid regions have been known for decades to have much less data than temperate
586 regions (Raich & Schlesinger, 1992) yet they continue to be underrepresented (Xu & Shang, 2016).
587 Arid regions are projected to expand and cover half of the globe by the end of the century (Huang
588 et al., 2016), making it crucial to monitor soil CO_2 efflux in dryland ecosystems.
589 **When?** The model consistently failed to capture the most extreme values, both low and high,
590 across many types of sites. Soil CO_2 efflux at some sites exhibits inherently complex and
591 temporally variable dynamics that are difficult for models to capture. For example, dryland
592 ecosystems experience drying-rewetting cycles that can cause hot moments in CO_2 efflux (Jarvis
593 et al., 2007); freeze-thaw cycles in cold climates can significantly increase dissolved organic
594 carbon availability and CO_2 efflux (Feng et al., 2007; Grogan et al., 2004; Herrmann & Witter,

2002; Song et al., 2017). These abrupt fluctuations, common in arid and cold regions, are expected to become more common in a changing climate (Blankinship & Hart, 2012; Gu et al., 2008; Henry, 2008; Meehl et al., 2006; Sheffield & Wood, 2008; Sinha & Cherkauer, 2010). Similarly, it is unclear how and how much extreme events like heatwaves, floods, and wildfires, which are becoming more frequent under climate change (Arnell & Gosling, 2016; Pausas & Keeley, 2021; Trenberth, 2011), will mobilize or suppress soil CO_2 efflux globally.

It is thus important to prioritize measurements that capture peaks and troughs in data, especially those caused by extreme weather events that often disproportionally change long-term soil CO_2 efflux dynamics (Vargas, 2012). To capture transient events and their implications, we need sufficient data to cover the full range of conditions in individual sites. On the other hand, stochastic events such as storms or rapid thaw, can repeatedly reset ecosystem states, preventing CO_2 efflux patterns from stabilizing into learnable patterns (Post & Knapp, 2020). In such cases, longer datasets may offer limited benefits, while finer-scale data capturing the timing and impacts of stochastic events could be more informative for improving model performance.

Peaks and troughs during extreme events can be particularly difficult to predict due to their rare occurrence and poorly-understood dynamics. However, deep learning models inherently learn patterns when provided with sufficient data. The key question is how much data is sufficient to adequately capture these dynamics. Whereas data during extreme events are always rare in individual sites, aggregating data during extreme events from hundreds to thousands of sites has shown promises for forecasting extreme events such as flooding (Bertola et al., 2023; Nearing et al., 2024).

4.4 What are the challenges beyond data scarcity?

Spatial and temporal scale discrepancy Model performance depends not only on target data availability but also the quality of predictor data (e.g., temperature, precipitation). If the predictor data used to train the model does not reflect variability in soil CO_2 efflux, more data will not improve model performance. One major issue in this model is the mismatch in spatial and temporal scales between predictor (e.g., temperature, precipitation) and target data (soil CO_2 efflux). For example, although soil CO_2 efflux data is at daily scale, normalized differential vegetation index (NDVI) has a four day resolution, evapotranspiration (ET) and potential evapotranspiration (PET) have an eight day resolution, and wind speed has a monthly resolution. This temporal mismatch could potentially "smooth out" the variability in predictor data that would meaningfully affect soil CO_2 efflux dynamics.

In addition, soil CO_2 efflux chamber measurements are at a meter scale, whereas global predictor data are mostly derived from remote sensing products at kilometer or coarser scales. As such, local variability in soil moisture, precipitation, and vegetation cover are likely averaged out in predictor data. Such scale discrepancy in data could have substantial impacts, especially where small-scale heterogeneity in soil moisture, precipitation, vegetation cover, or soil characteristics may play a disproportionally larger role than temperature in regulating CO_2 efflux (Bloom et al., 2016; Reichstein et al., 2019). Most notably, local moisture variations are averaged over around 11 square kilometers in the remote sensing data used in this model, making the predictor data used

here unlikely to represent local-scale precipitation/soil moisture variations. This could result in model prediction errors where soil CO_2 efflux is highly sensitive to soil moisture. For example, in arid regions with a pronounced dry season, soil rewetting and drying cycling can predominantly control soil CO_2 release (Almagro et al., 2009; Conant et al., 2000). In tropical regions with relatively steady temperatures, CO_2 efflux may be more responsive to precipitation, both positively (e.g., Chambers et al., 2004; Rubio & Detto, 2017) and negatively (Cleveland et al., 2010; Wieder et al., 2011). Within the same land cover or climate type, topographic position can suppress or mobilize soil CO_2 efflux by regulating local topographic wetness index or "wettability" (Riveros-Iregui & McGlynn, 2009).

More data sharing. In addition to new data acquisition, we also need to prioritize data sharing (Wolkovich et al., 2012). While there are many more sites with soil CO_2 efflux data than the 82 currently in COSORE, these data are not accessible and usable when not in a public dataset. The global carbon research community would greatly benefit from broader contributions to COSORE. Sharing these datasets would enable the application of advanced computational techniques to extract valuable insights and facilitate robust predictions for the future. Failing to upload such data is a missed opportunity to leverage them for large-scale data synthesis and predictive modeling.

5. CONCLUSION

Global-scale estimation of soil CO_2 efflux are mostly at the annual scale and thus miss sub-annual dynamics, potentially contributing to large estimation uncertainties. Here we develop a single deep learning model using daily data from 82 sites in COSORE, aiming to provide a steppingstone for predicting global daily soil CO_2 efflux. This model performs better in temperate and mesic sites with many data points and strong responses to temperature. Our results highlight challenges including temporal and spatial bias of target data and scale discrepancy between predictor and target data, underscoring the need to prioritize data collection in spatially underrepresented systems such as arid, Arctic/boreal, and tropical ecosystems and temporally underrepresented conditions such as extreme weather events that have become increasingly frequent and impactful. Nonetheless, the ability of the model to match daily-scale magnitude and dynamics across many diverse sites is promising. It holds the potential to reduce global estimation uncertainty, facilitate our understanding of daily to seasonal dynamics, to generate synthetic data to temporal and spatial gaps in temperate, mesic regions with good model performance, and to project into the future and the past. Deep learning models hold the potential to revolutionize global soil CO_2 efflux prediction and to generate testable mechanistic hypotheses about how processes are changing under climate change. But they will remain fundamentally limited in their predictive ability without greatly more equitable data collection.

Acknowledgements

The authors declare no competing interests. This work is supported by the United States Department of Energy DE-SC0025235.

Open Research

All predictor and target data and the code used to train the model can be found in a Zenodo repository at 10.5281/zenodo.149077.

References

Adachi, M., Ito, A., Yonemura, S., & Takeuchi, W. (2017). Estimation of global soil respiration by accounting for land-use changes derived from remote sensing data. Journal of Environmental Management, 200, 97–104. https://doi.org/10.1016/j.jenvman.2017.05.076

Almagro, M., López, J., Querejeta, J. I., & Martínez-Mena, M. (2009). Temperature dependence of soil CO2 efflux is strongly modulated by seasonal patterns of moisture availability in a Mediterranean ecosystem. Soil Biology and Biochemistry, 41(3), 594–605. https://doi.org/10.1016/j.soilbio.2008.12.021

Anjileli, H., Huning, L. S., Moftakhari, H., Ashraf, S., Asanjan, A. A., Norouzi, H., & AghaKouchak, A. (2021). Extreme heat events heighten soil respiration. Scientific Reports, 11(1), 6632. https://doi.org/10.1038/s41598-021-85764-8

Arain, M. A. (2016). AmeriFlux AmeriFlux CA-TPD Ontario - Turkey Point Mature Deciduous. Lawrence Berkeley National Laboratory (LBNL), Berkeley, CA (United States). AmeriFlux; McMaster Univ., Hamilton, ON (Canada). https://doi.org/10.17190/AMF/1246152

Arnell, N. W., & Gosling, S. N. (2016). The impacts of climate change on river flood risk at the global scale. Climatic Change, 134(3), 387–401. https://doi.org/10.1007/s10584-014-1084-5

Arora, V. K., Boer, G. J., Friedlingstein, P., Eby, M., Jones, C. D., Christian, J. R., et al. (2013). Carbon–Concentration and Carbon–Climate Feedbacks in CMIP5 Earth System Models. https://doi.org/10.1175/JCLI-D-12-00494.1

Ataka, M., Kominami, Y., Yoshimura, K., Miyama, T., Jomura, M., & Tani, M. (2014). In Situ CO2 Efflux from Leaf Litter Layer Showed Large Temporal Variation Induced by Rapid Wetting and Drying Cycle. PLOS ONE, 9(10), e108404. https://doi.org/10.1371/journal.pone.0108404

Ballantyne, A., Smith, W., Anderegg, W., Kauppi, P., Sarmiento, J., Tans, P., et al. (2017). Accelerating net terrestrial carbon uptake during the warming hiatus due to reduced respiration. Nature Climate Change, 7(2), 148–152. https://doi.org/10.1038/nclimate3204

Bauder, R. A., Khoshgoftaar, T. M., & Hasanin, T. (2018). An Empirical Study on Class Rarity in Big Data. In 2018 17th IEEE International Conference on Machine Learning and Applications (ICMLA) (pp. 785–790). https://doi.org/10.1109/ICMLA.2018.00125

Bernhardt, E. S., Blaszczak, J. R., Ficken, C. D., Fork, M. L., Kaiser, K. E., & Seybold, E. C. (2017). Control Points in Ecosystems: Moving Beyond the Hot Spot Hot Moment Concept. Ecosystems, 20(4), 665–682. https://doi.org/10.1007/s10021-016-0103-y

Bertola, M., Blöschl, G., Bohac, M., Borga, M., Castellarin, A., Chirico, G. B., et al. (2023). Megafloods in Europe can be anticipated from observations in hydrologically similar catchments. Nature Geoscience, 16(11), 982–988. https://doi.org/10.1038/s41561-023-01300-5

Blankinship, J. C., & Hart, S. C. (2012). Consequences of manipulated snow cover on soil gaseous emission and N retention in the growing season: a meta-analysis. Ecosphere, 3(1), art1. https://doi.org/10.1890/ES11-00225.1

Bloom, A. A., Exbrayat, J.-F., van der Velde, I. R., Feng, L., & Williams, M. (2016). The decadal state of the terrestrial carbon cycle: Global retrievals of terrestrial carbon allocation, pools, and residence times. Proceedings of the National Academy of Sciences, 113(5), 1285–1290. https://doi.org/10.1073/pnas.1515160113

Bond-Lamberty, B. (2018). New Techniques and Data for Understanding the Global Soil Respiration Flux. Earth's Future, 6(9), 1176–1180. https://doi.org/10.1029/2018EF000866

Bond-Lamberty, B., & Thomson, A. (2010). Temperature-associated increases in the global soil respiration record. Nature, 464(7288), 579–582. https://doi.org/10.1038/nature08930

Bond-Lamberty, B., Epron, D., Harden, J., Harmon, M. E., Hoffman, F., Kumar, J., et al. (2016). Estimating heterotrophic respiration at large scales: challenges, approaches, and next steps. Ecosphere, 7(6), e01380. https://doi.org/10.1002/ecs2.1380

Bond-Lamberty, B., Pennington, S. C., Jian, J., Megonigal, J. P., Sengupta, A., & Ward, N. (2019). Soil Respiration Variability and Correlation Across a Wide Range of Temporal Scales. Journal of Geophysical Research: Biogeosciences, 124(11), 3672–3683. https://doi.org/10.1029/2019JG005265

Bond-Lamberty, B., Christianson, D. S., Malhotra, A., Pennington, S. C., Sihi, D., AghaKouchak, A., et al. (2020). COSORE: A community database for continuous soil respiration and other soil-atmosphere greenhouse gas flux data. Global Change Biology, 26(12), 7268–7283. https://doi.org/10.1111/gcb.15353

Bond-Lamberty, B., Ballantyne, A., Berryman, E., Fluet-Chouinard, E., Jian, J., Morris, K. A., et al. (2024). Twenty Years of Progress, Challenges, and Opportunities in Measuring and Understanding Soil Respiration. Journal of Geophysical Research: Biogeosciences, 129(2), e2023JG007637. https://doi.org/10.1029/2023JG007637

Box, G. E. P., & Jenkins, G. M. (1976). Time Series Analysis: Forecasting and Control. Holden-Day.

Budyko, M. (1974). Climate and Life. Retrieved from https://shop.elsevier.com/books/climate-and-life/budyko/978-0-12-139450-9

Burbidge, J. B., Magee, L., & Robb, A. L. (1988). Alternative Transformations to Handle Extreme Values of the Dependent Variable. Journal of the American Statistical Association, 83(401), 123–127. https://doi.org/10.1080/01621459.1988.10478575

Burton, A. J., Pregitzer, K. S., Crawford, J. N., Zogg, G. P., & Zak, D. R. (2004). Simulated chronic NO3− deposition reduces soil respiration in northern hardwood forests. Global Change Biology, 10(7), 1080–1091. https://doi.org/10.1111/j.1365-2486.2004.00737.x

Carbone, M. S., & Vargas, R. (2008). Automated soil respiration measurements: new information, opportunities and challenges. New Phytologist, 177(2), 295–297. https://doi.org/10.1111/j.1469-8137.2007.02328.x

Carbone, Mariah S., Still, C. J., Ambrose, A. R., Dawson, T. E., Williams, A. P., Boot, C. M., et al. (2011). Seasonal and episodic moisture controls on plant and microbial contributions to soil respiration. Oecologia, 167(1), 265–278. https://doi.org/10.1007/s00442-011-1975-3

Carlyle, J. C., & Than, U. B. (1988). Abiotic Controls of Soil Respiration Beneath an Eighteen-Year-Old Pinus Radiata Stand in South-Eastern Australia. Journal of Ecology, 76(3), 654–662. https://doi.org/10.2307/2260565

Chambers, J. Q., Tribuzy, E. S., Toledo, L. C., Crispim, B. F., Higuchi, N., Santos, J. dos, et al. (2004). Respiration from a Tropical Forest Ecosystem: Partitioning of Sources and Low Carbon Use Efficiency. Ecological Applications, 14(sp4), 72–88. https://doi.org/10.1890/01-6012

Chang, Z., Feng, Q., Si, J., Su, Y., Xi, H., & Li, J. (2009). Analysis of the spatial and temporal changes in soil CO2 flux in alpine meadow of Qilian Mountain. Environmental Geology, 58(3), 483–490. https://doi.org/10.1007/s00254-008-1521-8

Chen, J., Dafflon, B., Tran, A. P., Falco, N., & Hubbard, S. S. (2021). A deep learning hybrid predictive modeling (HPM) approach for estimating evapotranspiration and ecosystem respiration. Hydrology and Earth System Sciences, 25(11), 6041–6066. https://doi.org/10.5194/hess-25-6041-2021

Chen, S., Wang, J., Zhang, T., & Hu, Z. (2020). Climatic, soil, and vegetation controls of the temperature sensitivity (Q10) of soil respiration across terrestrial biomes. Global Ecology and Conservation, 22, e00955. https://doi.org/10.1016/j.gecco.2020.e00955

Cleveland, C. C., Wieder, W. R., Reed, S. C., & Townsend, A. R. (2010). Experimental drought in a tropical rain forest increases soil carbon dioxide losses to the atmosphere. Ecology, 91(8), 2313–2323. https://doi.org/10.1890/09-1582.1

Conant, R. T., Klopatek, J. M., & Klopatek, C. C. (2000). Environmental Factors Controlling Soil Respiration in Three Semiarid Ecosystems. Soil Science Society of America Journal, 64(1), 383–390. https://doi.org/10.2136/sssaj2000.641383x

Desai, A. R., Murphy, B. A., Wiesner, S., Thom, J., Butterworth, B. J., Koupaei-Abyazani, N., et al. (2022). Drivers of Decadal Carbon Fluxes Across Temperate Ecosystems. Journal of Geophysical Research: Biogeosciences, 127(12), e2022JG007014. https://doi.org/10.1029/2022JG007014

Duiker, S. W., & Lal, R. (2000). Carbon budget study using CO2 flux measurements from a no till system in central Ohio. Soil and Tillage Research, 54(1), 21–30. https://doi.org/10.1016/S0167-1987(99)00101-4

Fang, K., Shen, C., Kifer, D., & Yang, X. (2017). Prolongation of SMAP to Spatiotemporally Seamless Coverage of Continental U.S. Using a Deep Learning Neural Network. Geophysical Research Letters, 44(21), 11,030-11,039. https://doi.org/10.1002/2017GL075619

Fang, K., Kifer, D., Lawson, K., Feng, D., & Shen, C. (2022). The Data Synergy Effects of Time-Series Deep Learning Models in Hydrology. Water Resources Research, 58(4), e2021WR029583. https://doi.org/10.1029/2021WR029583

Feng, D., Fang, K., & Shen, C. (2020). Enhancing Streamflow Forecast and Extracting Insights Using Long-Short Term Memory Networks With Data Integration at Continental Scales. Water Resources Research, 56(9), e2019WR026793. https://doi.org/10.1029/2019WR026793

Feng, D., Lawson, K., & Shen, C. (2021). Mitigating Prediction Error of Deep Learning Streamflow Models in Large Data-Sparse Regions With Ensemble Modeling and Soft Data. Geophysical Research Letters, 48(14), e2021GL092999. https://doi.org/10.1029/2021GL092999

Feng, X., Nielsen, L. L., & Simpson, M. J. (2007). Responses of soil organic matter and microorganisms to freeze–thaw cycles. Soil Biology and Biochemistry, 39(8), 2027–2037. https://doi.org/10.1016/j.soilbio.2007.03.003

Fick, S. E., & Hijmans, R. J. (2017). WorldClim 2: new 1-km spatial resolution climate surfaces for global land areas. International Journal of Climatology, 37(12), 4302–4315. https://doi.org/10.1002/joc.5086

Friedlingstein, P., O'Sullivan, M., Jones, M. W., Andrew, R. M., Hauck, J., Landschützer, P., et al. (2024). Global Carbon Budget 2024. Earth System Science Data Discussions, 1–133. https://doi.org/10.5194/essd-2024-519

Gaumont-Guay, D., Black, T. A., Barr, A. G., Griffis, T. J., Jassal, R. S., Krishnan, P., et al. (2014). Eight years of forest-floor CO2 exchange in a boreal black spruce forest: Spatial integration and long-term temporal trends. Agricultural and Forest Meteorology, 184, 25–35. https://doi.org/10.1016/j.agrformet.2013.08.010

van Gestel, N., Shi, Z., van Groenigen, K. J., Osenberg, C. W., Andresen, L. C., Dukes, J. S., et al. (2018). Predicting soil carbon loss with warming. Nature, 554(7693), E4–E5. https://doi.org/10.1038/nature25745

Gonzalez, P., Neilson, R. P., Lenihan, J. M., & Drapek, R. J. (2010). Global patterns in the vulnerability of ecosystems to vegetation shifts due to climate change. Global Ecology and Biogeography, 19(6), 755–768. https://doi.org/10.1111/j.1466-8238.2010.00558.x

Goulden, M. L., & Crill, P. M. (1997). Automated measurements of CO2 exchange at the moss surface of a black spruce forest. Tree Physiology, 17(8–9), 537–542. https://doi.org/10.1093/treephys/17.8-9.537

Greff, K., Srivastava, R. K., Koutník, J., Steunebrink, B. R., & Schmidhuber, J. (2017). LSTM: A Search Space Odyssey. IEEE Transactions on Neural Networks and Learning Systems, 28(10), 2222–2232. https://doi.org/10.1109/TNNLS.2016.2582924

Grogan, P., Michelsen, A., Ambus, P., & Jonasson, S. (2004). Freeze–thaw regime effects on carbon and nitrogen dynamics in sub-arctic heath tundra mesocosms. Soil Biology and Biochemistry, 36(4), 641–654. https://doi.org/10.1016/j.soilbio.2003.12.007

Gu, L., Hanson, P. J., Post, W. M., Kaiser, D. P., Yang, B., Nemani, R., et al. (2008). The 2007 Eastern US Spring Freeze: Increased Cold Damage in a Warming World? BioScience, 58(3), 253–262. https://doi.org/10.1641/B580311

Guenet, B., Orliac, J., Cécillon, L., Torres, O., Sereni, L., Martin, P. A., et al. (2024). Spatial biases reduce the ability of Earth system models to simulate soil heterotrophic respiration fluxes. Biogeosciences, 21(2), 657–669. https://doi.org/10.5194/bg-21-657-2024

Gupta, H. V., Kling, H., Yilmaz, K. K., & Martinez, G. F. (2009). Decomposition of the mean squared error and NSE performance criteria: Implications for improving hydrological modelling. Journal of Hydrology, 377(1), 80–91. https://doi.org/10.1016/j.jhydrol.2009.08.003

Gutiérrez del Arroyo, O., & Wood, T. E. (2020). Significant Diel Variation of Soil Respiration Suggests Aboveground and Belowground Controls in a Tropical Moist Forest in Puerto Rico. Journal of Geophysical Research: Biogeosciences, 125(3), e2019JG005353. https://doi.org/10.1029/2019JG005353

Haaf, D., Six, J., & Doetterl, S. (2021). Global patterns of geo-ecological controls on the response of soil respiration to warming. Nature Climate Change, 11(7), 623–627. https://doi.org/10.1038/s41558-021-01068-9

Hashimoto, S., Carvalhais, N., Ito, A., Migliavacca, M., Nishina, K., & Reichstein, M. (2015). Global spatiotemporal distribution of soil respiration modeled using a global database. Biogeosciences, 12(13), 4121–4132. https://doi.org/10.5194/bg-12-4121-2015

Hashimoto, Shoji, Ito, A., & Nishina, K. (2023). Divergent data-driven estimates of global soil respiration. Communications Earth & Environment, 4(1), 1–8. https://doi.org/10.1038/s43247-023-01136-2

Henry, H. A. L. (2008). Climate change and soil freezing dynamics: historical trends and projected changes. Climatic Change, 87(3), 421–434. https://doi.org/10.1007/s10584-007-9322-8

Herrmann, A., & Witter, E. (2002). Sources of C and N contributing to the flush in mineralization upon freeze–thaw cycles in soils. Soil Biology and Biochemistry, 34(10), 1495–1505. https://doi.org/10.1016/S0038-0717(02)00121-9

Hochreiter, S., & Schmidhuber, J. (1997). Long Short-term Memory. Neural Computation, 9, 1735–80. https://doi.org/10.1162/neco.1997.9.8.1735

howard, D. M., & howard, P. J. A. (1993). Relationships between co2 evolution, moisture content and temperature for a range of soil types. Soil Biology and Biochemistry, 25(11), 1537–1546. https://doi.org/10.1016/0038-0717(93)90008-Y

Huang, J., Yu, H., Guan, X., Wang, G., & Guo, R. (2016). Accelerated dryland expansion under climate change. Nature Climate Change, 6(2), 166–171. https://doi.org/10.1038/nclimate2837

Huang, N., Wang, L., Song, X.-P., Black, T. A., Jassal, R. S., Myneni, R. B., et al. (2020). Spatial and temporal variations in global soil respiration and their relationships with climate and land cover. Science Advances, 6(41), eabb8508. https://doi.org/10.1126/sciadv.abb8508

Irvine, J., & Law, B. E. (2002). Contrasting soil respiration in young and old-growth ponderosa pine forests. Global Change Biology, 8(12), 1183–1194. https://doi.org/10.1046/j.1365-2486.2002.00544.x

Janssens, I. A., Lankreijer, H., Matteucci, G., Kowalski, A. S., Buchmann, N., Epron, D., et al. (2001). Productivity overshadows temperature in determining soil and ecosystem respiration across European forests. Global Change Biology, 7(3), 269–278. https://doi.org/10.1046/j.1365-2486.2001.00412.x

871 Janssens, Ivan A., Barigah, S. T., & Ceulemans, R. (1998). Soil CO2 efflux rates in different
872 tropical vegetation types in French Guiana. Annales Des Sciences Forestières, 55(6), 671–680.
873 https://doi.org/10.1051/forest:19980603
874 Jarvis, P., Rey, A., Petsikos, C., Wingate, L., Rayment, M., Pereira, J., et al. (2007). Drying and
875 wetting of Mediterranean soils stimulates decomposition and carbon dioxide emission: the
876 "Birch effect." Tree Physiology, 27(7), 929–940. https://doi.org/10.1093/treephys/27.7.929
877 Jian, J., Steele, M. K., Thomas, R. Q., Day, S. D., & Hodges, S. C. (2018). Constraining
878 estimates of global soil respiration by quantifying sources of variability. Global Change Biology,
879 24(9), 4143–4159. https://doi.org/10.1111/gcb.14301
880 Jian, J., Bailey, V., Dorheim, K., Konings, A. G., Hao, D., Shiklomanov, A. N., et al. (2022).
881 Historically inconsistent productivity and respiration fluxes in the global terrestrial carbon cycle.
882 Nature Communications, 13(1), 1733. https://doi.org/10.1038/s41467-022-29391-5
883 Jiang, J., Feng, L., Hu, J., Liu, H., Zhu, C., Chen, B., & Chen, T. (2024). Global soil respiration
884 predictions with associated uncertainties from different spatio-temporal data subsets. Ecological
885 Informatics, 82, 102777. https://doi.org/10.1016/j.ecoinf.2024.102777
886 Jiang, P., Chen, X., Missik, J. E. C., Gao, Z., Liu, H., & Verbeke, B. A. (2022). Encoding diel
887 hysteresis and the Birch effect in dryland soil respiration models through knowledge-guided deep
888 learning. Frontiers in Environmental Science, 10. Retrieved from
889 https://www.frontiersin.org/articles/10.3389/fenvs.2022.1035540
890 Johnson, J. M., & Khoshgoftaar, T. M. (2019). Survey on deep learning with class imbalance.
891 Journal of Big Data, 6(1), 27. https://doi.org/10.1186/s40537-019-0192-5
892 Kätterer, T., Reichstein, M., Andrén, O., & Lomander, A. (1998). Temperature dependence of
893 organic matter decomposition: a critical review using literature data analyzed with different
894 models. Biology and Fertility of Soils, 27(3), 258–262. https://doi.org/10.1007/s003740050430
895 Kim, D.-G., Bond-Lamberty, B., Ryu, Y., Seo, B., & Papale, D. (2022). Ideas and perspectives:
896 Enhancing research and monitoring of carbon pools and land-to-atmosphere greenhouse gases
897 exchange in developing countries. Biogeosciences, 19(5), 1435–1450.
898 https://doi.org/10.5194/bg-19-1435-2022
899 Kirschbaum, M. U. F. (1995). The temperature dependence of soil organic matter decomposition,
900 and the effect of global warming on soil organic C storage. Soil Biology and Biochemistry,
901 27(6), 753–760. https://doi.org/10.1016/0038-0717(94)00242-S
902 Knoben, W. J. M., Freer, J. E., & Woods, R. A. (2019). Technical note: Inherent benchmark or
903 not? Comparing Nash–Sutcliffe and Kling–Gupta efficiency scores. Hydrology and Earth
904 System Sciences, 23(10), 4323–4331. https://doi.org/10.5194/hess-23-4323-2019
905 Kratzert, F., Klotz, D., Brenner, C., Schulz, K., & Herrnegger, M. (2018). Rainfall–runoff
906 modelling using Long Short-Term Memory (LSTM) networks. Hydrology and Earth System
907 Sciences, 22(11), 6005–6022. https://doi.org/10.5194/hess-22-6005-2018
908 Kratzert, F., Klotz, D., Shalev, G., Klambauer, G., Hochreiter, S., & Nearing, G. (2019).
909 Towards learning universal, regional, and local hydrological behaviors via machine learning

applied to large-sample datasets. Hydrology and Earth System Sciences, 23(12), 5089–5110. https://doi.org/10.5194/hess-23-5089-2019

Kratzert, F., Nearing, G., Addor, N., Erickson, T., Gauch, M., Gilon, O., et al. (2023). Caravan - A global community dataset for large-sample hydrology. Scientific Data, 10(1), 61. https://doi.org/10.1038/s41597-023-01975-w

Le, V. H., & Vargas, R. (2024). Beyond a deterministic representation of the temperature dependence of soil respiration. Science of The Total Environment, 912, 169391. https://doi.org/10.1016/j.scitotenv.2023.169391

Lei, J., Guo, X., Zeng, Y., Zhou, J., Gao, Q., & Yang, Y. (2021). Temporal changes in global soil respiration since 1987. Nature Communications, 12(1), 403. https://doi.org/10.1038/s41467-020-20616-z

Liang, N., Teramoto, M., Takagi, M., & Zeng, J. (2017). High-resolution data on the impact of warming on soil CO2 efflux from an Asian monsoon forest. Scientific Data, 4(1), 170026. https://doi.org/10.1038/sdata.2017.26

Liu, J., Rahmani, F., Lawson, K., & Shen, C. (2022). A Multiscale Deep Learning Model for Soil Moisture Integrating Satellite and In Situ Data. Geophysical Research Letters, 49(7), e2021GL096847. https://doi.org/10.1029/2021GL096847

Liu, J., Bian, Y., Lawson, K., & Shen, C. (2024). Probing the limit of hydrologic predictability with the Transformer network. Journal of Hydrology, 637, 131389. https://doi.org/10.1016/j.jhydrol.2024.131389

Lloyd, J., & Taylor, J. A. (1994). On the Temperature Dependence of Soil Respiration. Functional Ecology, 8(3), 315–323. https://doi.org/10.2307/2389824

Loveland, T. R., Reed, B. C., Brown, J. F., Ohlen, D. O., Zhu, Z., Yang, L., & Merchant, J. W. (2000). Development of a global land cover characteristics database and IGBP DISCover from 1 km AVHRR data. International Journal of Remote Sensing, 21(6–7), 1303–1330. https://doi.org/10.1080/014311600210191

Luo, Y., & Zhou, X. (2006). Soil Respiration and the Environment. Elsevier Inc. https://doi.org/10.1016/B978-0-12-088782-8.X5000-1

MacKinnon, J. G., & Magee, L. (1990). Transforming the Dependent Variable in Regression Models. International Economic Review, 31(2), 315–339. https://doi.org/10.2307/2526842

Martin, L. J., Blossey, B., & Ellis, E. (2012). Mapping where ecologists work: biases in the global distribution of terrestrial ecological observations. Frontiers in Ecology and the Environment, 10(4), 195–201. https://doi.org/10.1890/110154

McClain, M. E., Boyer, E. W., Dent, C. L., Gergel, S. E., Grimm, N. B., Groffman, P. M., et al. (2003). Biogeochemical Hot Spots and Hot Moments at the Interface of Terrestrial and Aquatic Ecosystems. Ecosystems, 6(4), 301–312. https://doi.org/10.1007/s10021-003-0161-9

Meehl, G. A., Arblaster, J. M., Lawrence, D. M., Seth, A., Schneider, E. K., Kirtman, B. P., & Min, D. (2006). Monsoon Regimes in the CCSM3. Journal of Climate, 19(11), 2482–2495. https://doi.org/10.1175/JCLI3745.1

Metz, E.-M., Vardag, S. N., Basu, S., Jung, M., Ahrens, B., El-Madany, T., et al. (2023). Soil respiration–driven CO2 pulses dominate Australia's flux variability. Science, 379(6639), 1332–1335. https://doi.org/10.1126/science.add7833

Meyer, N., Welp, G., & Amelung, W. (2018). The Temperature Sensitivity (Q10) of Soil Respiration: Controlling Factors and Spatial Prediction at Regional Scale Based on Environmental Soil Classes. Global Biogeochemical Cycles, 32(2), 306–323. https://doi.org/10.1002/2017GB005644

Misson, L., Rocheteau, A., Rambal, S., Ourcival, J.-M., Limousin, J.-M., & Rodriguez, R. (2010). Functional changes in the control of carbon fluxes after 3 years of increased drought in a Mediterranean evergreen forest? Global Change Biology, 16(9), 2461–2475. https://doi.org/10.1111/j.1365-2486.2009.02121.x

Nash, J. E., & Sutcliffe, J. V. (1970). River flow forecasting through conceptual models part I — A discussion of principles. Journal of Hydrology, 10(3), 282–290. https://doi.org/10.1016/0022-1694(70)90255-6

Nearing, G., Cohen, D., Dube, V., Gauch, M., Gilon, O., Harrigan, S., et al. (2024). Global prediction of extreme floods in ungauged watersheds. Nature, 627(8004), 559–563. https://doi.org/10.1038/s41586-024-07145-1

Nearing, G. S., Kratzert, F., Sampson, A. K., Pelissier, C. S., Klotz, D., Frame, J. M., et al. (2021). What Role Does Hydrological Science Play in the Age of Machine Learning? Water Resources Research, 57(3), e2020WR028091. https://doi.org/10.1029/2020WR028091

Nissan, A., Alcolombri, U., Peleg, N., Galili, N., Jimenez-Martinez, J., Molnar, P., & Holzner, M. (2023). Global warming accelerates soil heterotrophic respiration. Nature Communications, 14(1), 3452. https://doi.org/10.1038/s41467-023-38981-w

Norman, J. M., Garcia, R., & Verma, S. B. (1992). Soil surface CO2 fluxes and the carbon budget of a grassland. Journal of Geophysical Research: Atmospheres, 97(D17), 18845–18853. https://doi.org/10.1029/92JD01348

Pausas, J. G., & Keeley, J. E. (2021). Wildfires and global change. Frontiers in Ecology and the Environment, 19(7), 387–395. https://doi.org/10.1002/fee.2359

Perry, G. L. W., Seidl, R., Bellvé, A. M., & Rammer, W. (2022). An Outlook for Deep Learning in Ecosystem Science. Ecosystems, 25(8), 1700–1718. https://doi.org/10.1007/s10021-022-00789-y

Phillips, C. L., Murphey, V., Lajtha, K., & Gregg, J. W. (2016). Asymmetric and symmetric warming increases turnover of litter and unprotected soil C in grassland mesocosms. Biogeochemistry, 128(1), 217–231. https://doi.org/10.1007/s10533-016-0204-x

Poggio, L., de Sousa, L. M., Batjes, N. H., Heuvelink, G. B. M., Kempen, B., Ribeiro, E., & Rossiter, D. (2021). SoilGrids 2.0: producing soil information for the globe with quantified spatial uncertainty. SOIL, 7(1), 217–240. https://doi.org/10.5194/soil-7-217-2021

Post, A. K., & Knapp, A. K. (2020). The importance of extreme rainfall events and their timing in a semi-arid grassland. Journal of Ecology, 108(6), 2431–2443. https://doi.org/10.1111/1365-2745.13478

Raich, J. W., & Schlesinger, W. H. (1992). The global carbon dioxide flux in soil respiration and its relationship to vegetation and climate. Tellus B, 44(2), 81–99. https://doi.org/10.1034/j.1600-0889.1992.t01-1-00001.x

Raich, James W., & Potter, C. S. (1995). Global patterns of carbon dioxide emissions from soils. Global Biogeochemical Cycles, 9(1), 23–36. https://doi.org/10.1029/94GB02723

Raich, James W., Potter, C. S., & Bhagawati, D. (2002). Interannual variability in global soil respiration, 1980–94. Global Change Biology, 8(8), 800–812. https://doi.org/10.1046/j.1365-2486.2002.00511.x

Rantanen, M., Karpechko, A. Y., Lipponen, A., Nordling, K., Hyvärinen, O., Ruosteenoja, K., et al. (2022). The Arctic has warmed nearly four times faster than the globe since 1979. Communications Earth & Environment, 3(1), 1–10. https://doi.org/10.1038/s43247-022-00498-3

Rayment, M. B., & Jarvis, P. G. (1997). An improved open chamber system for measuring soil CO2 effluxes in the field. Journal of Geophysical Research: Atmospheres, 102(D24), 28779–28784. https://doi.org/10.1029/97JD01103

Reichstein, M., Bednorz, F., Broll, G., & Kätterer, T. (2000). Temperature dependence of carbon mineralisation: conclusions from a long-term incubation of subalpine soil samples. Soil Biology and Biochemistry, 32(7), 947–958. https://doi.org/10.1016/S0038-0717(00)00002-X

Reichstein, M., Camps-Valls, G., Stevens, B., Jung, M., Denzler, J., Carvalhais, N., & Prabhat. (2019). Deep learning and process understanding for data-driven Earth system science. Nature, 566(7743), 195–204. https://doi.org/10.1038/s41586-019-0912-1

Rey, A. (2015). Mind the gap: non-biological processes contributing to soil CO2 efflux. Global Change Biology, 21(5), 1752–1761. https://doi.org/10.1111/gcb.12821

Riveros-Iregui, D. A., & McGlynn, B. L. (2009). Landscape structure control on soil CO2 efflux variability in complex terrain: Scaling from point observations to watershed scale fluxes. Journal of Geophysical Research: Biogeosciences, 114(G2). https://doi.org/10.1029/2008JG000885

Rubio, V. E., & Detto, M. (2017). Spatiotemporal variability of soil respiration in a seasonal tropical forest. Ecology and Evolution, 7(17), 7104–7116. https://doi.org/10.1002/ece3.3267

Savage, K., Phillips, R., & Davidson, E. (2014). High temporal frequency measurements of greenhouse gas emissions from soils. Biogeosciences, 11(10), 2709–2720. https://doi.org/10.5194/bg-11-2709-2014

Schlesinger, W. H. (1977). Carbon Balance in Terrestrial Detritus. Annual Review of Ecology, Evolution, and Systematics, 8(Volume 8, 1977), 51–81. https://doi.org/10.1146/annurev.es.08.110177.000411

Sheffield, J., & Wood, E. F. (2008). Projected changes in drought occurrence under future global warming from multi-model, multi-scenario, IPCC AR4 simulations. Climate Dynamics, 31(1), 79–105. https://doi.org/10.1007/s00382-007-0340-z

Shen, C. (2018). A Transdisciplinary Review of Deep Learning Research and Its Relevance for Water Resources Scientists. Water Resources Research, 54(11), 8558–8593. https://doi.org/10.1029/2018WR022643

Shen, C., Appling, A. P., Gentine, P., Bandai, T., Gupta, H., Tartakovsky, A., et al. (2023). Differentiable modelling to unify machine learning and physical models for geosciences. Nature Reviews Earth & Environment, 4(8), 552–567. https://doi.org/10.1038/s43017-023-00450-9

Shiff, S., Helman, D., & Lensky, I. M. (2021). Worldwide continuous gap-filled MODIS land surface temperature dataset. Scientific Data, 8(1), 74. https://doi.org/10.1038/s41597-021-00861-7

Sihi, D., Davidson, E. A., Chen, M., Savage, K. E., Richardson, A. D., Keenan, T. F., & Hollinger, D. Y. (2018). Merging a mechanistic enzymatic model of soil heterotrophic respiration into an ecosystem model in two AmeriFlux sites of northeastern USA. Agricultural and Forest Meteorology, 252, 155–166. https://doi.org/10.1016/j.agrformet.2018.01.026

Singh, J. S., & Gupta, S. R. (1977). Plant decomposition and soil respiration in terrestrial ecosystems. The Botanical Review, 43(4), 449–528. https://doi.org/10.1007/BF02860844

Sinha, T., & Cherkauer, K. A. (2010). Impacts of future climate change on soil frost in the midwestern United States. Journal of Geophysical Research: Atmospheres, 115(D8). https://doi.org/10.1029/2009JD012188

Song, Q.-H., Tan, Z.-H., Zhang, Y.-P., Cao, M., Sha, L.-Q., Tang, Y., et al. (2013). Spatial heterogeneity of soil respiration in a seasonal rainforest with complex terrain. iForest - Biogeosciences and Forestry, 6(2), 65. https://doi.org/10.3832/ifor0681-006

Song, Y., Zou, Y., Wang, G., & Yu, X. (2017). Altered soil carbon and nitrogen cycles due to the freeze-thaw effect: A meta-analysis. Soil Biology and Biochemistry, 109, 35–49. https://doi.org/10.1016/j.soilbio.2017.01.020

Stell, E., Warner, D., Jian, J., Bond-Lamberty, B., & Vargas, R. (2021). Spatial biases of information influence global estimates of soil respiration: How can we improve global predictions? Global Change Biology, 27(16), 3923–3938. https://doi.org/10.1111/gcb.15666

Sterle, G., Perdrial, J., Kincaid, D. W., Underwood, K. L., Rizzo, D. M., Haq, I. U., et al. (2024). CAMELS-Chem: augmenting CAMELS (Catchment Attributes and Meteorology for Large-sample Studies) with atmospheric and stream water chemistry data. Hydrology and Earth System Sciences, 28(3), 611–630. https://doi.org/10.5194/hess-28-611-2024

Thomey, M. L., Collins, S. L., Vargas, R., Johnson, J. E., Brown, R. F., Natvig, D. O., & Friggens, M. T. (2011). Effect of precipitation variability on net primary production and soil respiration in a Chihuahuan Desert grassland. Global Change Biology, 17(4), 1505–1515. https://doi.org/10.1111/j.1365-2486.2010.02363.x

Trenberth, K. (2011). Changes in precipitation with climate change. Climate Research, 47(1), 123–138. https://doi.org/10.3354/cr00953

Vargas, R. (2012). How a hurricane disturbance influences extreme CO2 fluxes and variance in a tropical forest. Environmental Research Letters, 7(3), 035704. https://doi.org/10.1088/1748-9326/7/3/035704

Vargas, R., & Allen, M. F. (2008). Environmental controls and the influence of vegetation type, fine roots and rhizomorphs on diel and seasonal variation in soil respiration. New Phytologist, 179(2), 460–471. https://doi.org/10.1111/j.1469-8137.2008.02481.x

Vargas, R., Detto, M., Baldocchi, D. D., & Allen, M. F. (2010). Multiscale analysis of temporal variability of soil CO2 production as influenced by weather and vegetation. Global Change Biology, 16(5), 1589–1605. https://doi.org/10.1111/j.1365-2486.2009.02111.x

Vargas, R., Carbone, M. S., Reichstein, M., & Baldocchi, D. D. (2011). Frontiers and challenges in soil respiration research: from measurements to model-data integration. Biogeochemistry, 102(1), 1–13. https://doi.org/10.1007/s10533-010-9462-1

Vargas, R., Sánchez-Cañete P., E., Serrano-Ortiz, P., Curiel Yuste, J., Domingo, F., López-Ballesteros, A., & Oyonarte, C. (2018). Hot-Moments of Soil CO2 Efflux in a Water-Limited Grassland. Soil Systems, 2(3), 47. https://doi.org/10.3390/soilsystems2030047

Varney, R. M., Chadburn, S. E., Burke, E. J., & Cox, P. M. (2022). Evaluation of soil carbon simulation in CMIP6 Earth system models. Biogeosciences, 19(19), 4671–4704. https://doi.org/10.5194/bg-19-4671-2022

Villarreal, S., & Vargas, R. (2021). Representativeness of FLUXNET Sites Across Latin America. Journal of Geophysical Research: Biogeosciences, 126(3), e2020JG006090. https://doi.org/10.1029/2020JG006090

Villarreal, S., Guevara, M., Alcaraz-Segura, D., & Vargas, R. (2019). Optimizing an Environmental Observatory Network Design Using Publicly Available Data. Journal of Geophysical Research: Biogeosciences, 124(7), 1812–1826. https://doi.org/10.1029/2018JG004714

Wang, J., Teng, D., He, X., Qin, L., Yang, X., & Lv, G. (2021). Spatial non-stationarity effects of driving factors on soil respiration in an arid desert region. CATENA, 207, 105617. https://doi.org/10.1016/j.catena.2021.105617

Warner, D. L., Bond-Lamberty, B., Jian, J., Stell, E., & Vargas, R. (2019). Spatial Predictions and Associated Uncertainty of Annual Soil Respiration at the Global Scale. Global Biogeochemical Cycles, 33(12), 1733–1745. https://doi.org/10.1029/2019GB006264

Wieder, W. R., Cleveland, C. C., & Townsend, A. R. (2011). Throughfall exclusion and leaf litter addition drive higher rates of soil nitrous oxide emissions from a lowland wet tropical forest. Global Change Biology, 17(10), 3195–3207. https://doi.org/10.1111/j.1365-2486.2011.02426.x

Wolkovich, E. M., Regetz, J., & O'Connor, M. I. (2012). Advances in global change research require open science by individual researchers. Global Change Biology, 18(7), 2102–2110. https://doi.org/10.1111/j.1365-2486.2012.02693.x

Wood, T. E., Detto, M., & Silver, W. L. (2013). Sensitivity of Soil Respiration to Variability in Soil Moisture and Temperature in a Humid Tropical Forest. PLoS ONE, 8(12), e80965. https://doi.org/10.1371/journal.pone.0080965

Wu, J., Pang, Z., Sun, T., Kan, H., Hu, W., & Li, X. (2016). Soil respiration simulation based on soil temperature and water content in artificial smooth brome grassland. The Rangeland Journal, 38(6), 579–589. https://doi.org/10.1071/RJ16023

Wutzler, T., Perez-Priego, O., Morris, K., El-Madany, T. S., & Migliavacca, M. (2020). Soil CO2 efflux errors are lognormally distributed – implications and guidance. Geoscientific

Instrumentation, Methods and Data Systems, 9(1), 239–254. https://doi.org/10.5194/gi-9-239-2020

Xu, M., & Shang, H. (2016). Contribution of soil respiration to the global carbon equation. Journal of Plant Physiology, 203, 16–28. https://doi.org/10.1016/j.jplph.2016.08.007

Yao, R., Wang, L., Huang, X., Cao, Q., Wei, J., He, P., et al. (2023). Global seamless and high-resolution temperature dataset (GSHTD), 2001–2020. Remote Sensing of Environment, 286, 113422. https://doi.org/10.1016/j.rse.2022.113422

Zhang, Z., Li, Y., Williams, R. A., Chen, Y., Peng, R., Liu, X., et al. (2023). Responses of soil respiration and its sensitivities to temperature and precipitation: A meta-analysis. Ecological Informatics, 75, 102057. https://doi.org/10.1016/j.ecoinf.2023.102057

Zhao, Z., Peng, C., Yang, Q., Meng, F.-R., Song, X., Chen, S., et al. (2017). Model prediction of biome-specific global soil respiration from 1960 to 2012. Earth's Future, 5(7), 715–729. https://doi.org/10.1002/2016EF000480

Zhi, W., Klingler, C., Liu, J., & Li, L. (2023). Widespread deoxygenation in warming rivers. Nature Climate Change, 13(10), 1105–1113. https://doi.org/10.1038/s41558-023-01793-3

Zhou, T., Shi, P., Hui, D., & Luo, Y. (2009). Global pattern of temperature sensitivity of soil heterotrophic respiration (Q10) and its implications for carbon-climate feedback. Journal of Geophysical Research: Biogeosciences, 114(G2). https://doi.org/10.1029/2008JG000850

SUPPLEMENTARY INFORMATION

Table 1: Summary of remote sensing data used in this work

Predictor	Source	Bands	Spatial resolution	Temporal resolution	Units	Access
Precipitation	ECMWF Climate Reanalysis ERA5 Land	precipitation	11132 m	Hourly, summed to daily scale	m	https://doi.org/10.24381/cds.68d2bb30
Soil Moisture	ECMWF Climate Reanalysis ERA5 Land	volumetric_soil_water_layer_1 volumetric_soil_water_layer_1			Volume fraction	https://doi.org/10.24381/cds.68d2bb30
Temperature	MOD21A1D.061 Aqua	LST_Day_1km	1000 m	Daily	K	https://doi.org/10.5067/MODIS/MYD21A1D.061

Minimum/Maximum Temperature	Global Seamless High-resolution Temperature Dataset (GSHTD)	TMIN TMAX	1000 m	Daily	K	https://doi.org/10.1016/j.rse.2022.113422
NDVI	LANDSAT 7 Level 2, Collection 2, Tier 1	SR_B3 SR_B4	30 m	Monthly	N/A	https://doi.org/10.7289/V5ZG6QH9
Evapotranspiration (ET)	MOD16A2GF.061 Terra	ET ET_QC	500 m	8-day	mm/8day	https://doi.org/10.5067/MODIS/MOD16A2GF.061
Potential Evapotranspiration (PET)	MOD16A2GF.061 Terra	PET ET_QC	500 m	8-day	mm/8day	https://doi.org/10.5067/MODIS/MOD16A2GF.061
Fraction of photosynthetically active radiation (FPAR)	MCD15A3H.061	Fpar	500 m	4-day	nm	https://doi.org/10.5067/MODIS/MCD15A3H.061
Leaf area index (LAI)	MCD15A3H.061	Lai	500 m	4-day	nm	https://doi.org/10.5067/MODIS/MCD15A3H.061
Clay, sand, and silt content; bulk density; soil organic carbon content	SoilGrids	soc sand silt clay bdod	250 m	N/A	g/kg % % % kg/dm^3	https://doi.org/10.5194/soil-7-217-2021
Mean annual temperature & precipitation (MAT &	WorldClim Version 2	N/A	1000 m	Annual	°C Cm/yr	https://doi.org/10.1002/joc.5086

MAP)						

$$x_t = ReLU(W_I I_t + b_t) \quad (1.1)$$

$$f_t = \sigma(W_{fx} x_t + U_{fh} h_{t-1} + b_f) \quad (1.2)$$

$$i_t = \sigma(W_{ix} x_t + U_{ih} h_{t-1} + b_i) \quad (1.3)$$

$$g_t = tanh(W_{gx} x_t + U_{gh} h_{t-1} + b_g) \quad (1.4)$$

$$o_t = \sigma(W_{ox} x_t + U_{oh} h_{t-1} + b_o) \quad (1.5)$$

$$c_t = f_t \cdot c_{t-1} + i_t \cdot g_t \quad (1.6)$$

$$h_t = tanh(c_t) \cdot o_t \quad (1.7)$$

$$y_t = W_{hy} h_t + b_y \quad (1.8)$$